Electronic Supplementary Material (ESI) for Environmental Science: Nano.

Supporting Information For:

Regulating Water Decontamination and Food Safety by a Reusable, Nanosized MOF@Cotton@Chitosan Composite Through Nanomolar Detection of Drug Nitroxinil and Organoarsenic Feed Additive *p*-Arsanilic Acid

*Subhrajyoti Ghosh, Debjit Mal and Shyam Biswas**

Department of Chemistry, Indian Institute of Technology Guwahati, 781039 Assam, India

*Corresponding author. Tel: 91-3612583309, Fax: 91-3612582349

E-mail address: sbiswas@iitg.ac.in

Materials and Characterization Methods:

All the reagents, starting materials and solvents were procured from commercial sources and used without purification, except the 2-formamidoterephthalic acid ligand (H_2BDC-NH-CHO). The ligand synthesis procedure is discussed below (Scheme S1) and its purity was verified by the FT-IR, ^{1}H NMR, ^{13}C NMR and mass spectrometric analysis (Figures S1-S3). The notations used for characterization of the bands are broad (br), strong (s), very strong (vs), medium (m), weak (w) and shoulder (sh). PXRD data were collected by using Rigaku Smartlab X-ray diffractometer with Cu-*K*α radiation (l = 1.54056 Å), 40 kV of operating voltage and 125 mA of operating current. Fourier transform infrared spectroscopy was performed in the region 400–4000 cm^{-1} with a PerkinElmer Spectrum Two FT-IR spectrometer. Thermogravimetric analysis (TGA) was carried out with a PerkinElmer TGA 4000 thermogravimetric analyser in the temperature range of 30-700 °C in O_2 atmosphere at the rate of 4 °C min^{-1}. N_2 sorption isotherms were recorded by using Quantachrome Autosorb iQ-MP volumetric gas adsorption equipment at -196 °C. Before the sorption analysis, the degassing of the compound was carried out at 100 °C under a high vacuum for 24 h. Fluorescence sensing studies were performed with a HORIBA JOBIN YVON Fluoromax-4 spectrofluorometer. FE-SEM images were captured with a Zeiss (Zemini) scanning electron microscope. A Bruker Avance III 500 NMR spectrometer was used for recording ^{1}H NMR spectra at 500 MHz. Mass spectra were recorded with an Agilent 6520 QTOF high-resolution mass spectrometer (HR-MS). Fluorescence lifetimes were measured using Picosecond Time-resolved and Steady State Luminescence Spectrometer on an Edinburg Instruments Lifespec II & FSP 920 instrument. Pawley refinement was carried out using Materials Studio software. The DICVOL program incorporated within STOE's WinXPow software package was used to determine the lattice parameters.

Synthesis of H_2BDC-NH-CHO Ligand:

At first, 6 mmol (1086 mg) of 2-aminoterephthalic acid and 24 mL of toluene were poured into a 50 mL of round bottom flask and 400 µL of conc. HCl was added into it. It was followed by the addition of 2 mL of formamide solution. Then, the reaction mixture was heated at 120 °C for 24 h with continuous stirring (Scheme S1). After that, excess ice-cold water was added to the reaction mixture, resulting in white precipitation. Thereafter, the obtained solid product (H_2BDC-NH-CHO) was filtered, washed with a large amount of water and dried in an oven at 60 °C. Yield: 870 mg (4.2 mmol, 69%). ^{1}H NMR (500 MHz, DMSO-d_6): 11.04 (d, 1H), 9.10 (s, 1H), 8.54 (s, 1H), 8.07 (d, 1H), 7.70 (d, 1H), ^{13}C NMR (125 MHz, DMSO-d_6) 166.98, 166.95, 160.88, 149.06, 146.78, 136.58, 128.73, 126.99, 125.92 ppm. HR-MS (m/z): 208.0257 for $(M+H)^-$ ion (M = mass of H_2BDC-NH-CHO ligand). In Figures S1-S3, the NMR and mass spectra of the H_2BDC-NH-CHO ligand are shown.

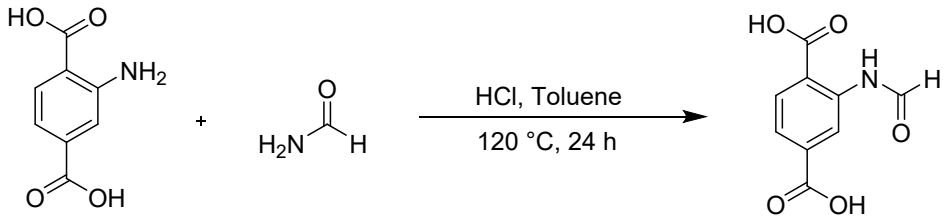

Scheme S1. Reaction scheme for the preparation of H_2BDC-NH-CHO ligand.

Preparation of MOF (1′) Suspension for the Fluorescence Sensing Experiments:

The probe **1′** (3 mg) was taken in a 5 mL glass vial containing 3 mL deionized water. Then, the suspension was sonicated for 15 min and kept it for overnight to make the suspension stable. During the fluorescence experiment, 200 µL of above-mentioned suspension of **1′** was added to 3000 µL of deionized water in a quartz cuvette. All the fluorescence spectra were collected in the range of 390-550 nm by exciting the suspension at 370 nm. For competitive experiments, the solutions of the different competitive analytes (concentration = 10 mM for NX sensing and 5 mM for PAA sensing) were added to the suspension of **1′** and spectra were collected in the same range.

Sensing of NX in Blood Serum Samples:

10 mL of blood sample was collected from the right arm vein of a healthy person (blood group A^+) and the blood plasma was separated by centrifuging the sample at 10,000 rpm for 15 min. The light-yellow blood serum was collected in a Falcon tube and stored at -20 °C in a refrigerator. For fluorescence detection experiments, aliquots of different concentrations of NX were spiked into the blood serum sample, which contained HEPES buffer suspension of the MOF.

Sensing of NX in Urine Samples:

10 mL of the first morning urine sample from a healthy person was taken and 500 mL of HNO_3 was added to the sample to kill any interfering living things. The sample was centrifuged at 8000 rpm for 10 min. For the further experiments, the supernatants were taken. Different NX aliquots were added into urine samples containing HEPES buffer suspensions of the probe.

Fabrication of MOF@Chitosan@Cotton Composite:

To fabricate the composite, initially, 50 mg of chitosan was stirred in 10 mL of water after adding 300 µL of glacial acetic acid in a test tube. After preparing this homogeneous chitosan solution, 200 mg of solid MOF was added to it and sonicated for 30 min to disperse the MOF particles homogeneously in the polymeric solution. After that, ten pieces (1 ×1 cm^2) of cotton fabric were dipped into that pale yellow-coloured suspension and then it was dried in an 80 °C oven. This process was repeated three times to coat the polymeric solution uniformly.

Analysis of Band Gap:

For **1′**: E_g = 2.79 eV (calculated from the Tauc plot, Figure S64a)

E_{VB} = Width of the He I UPS spectra from the excitation energy (21.22 eV)
E_{VB} = 21.22 - (18.62 – 4.33) = 6.93 eV
$E_{CB} = E_{VB} - E_g$ = 4.14 eV
With respect to RHE:
E_{VB} = 6.93 - 4.44 = 2.49 V
E_{CB} = 4.14 - 4.44 = -0.30 V

For NX: E_g = 3.63 eV (calculated from the Tauc plot, Figure S64b)
E_{VB} = Width of the He I UPS spectra from the excitation energy (21.22 eV)
E_{VB} = 21.22 - (17.32 – 4.58) = 8.48 eV
$E_{CB} = E_{VB} - E_g$ = 4.85 eV
With respect to RHE:
E_{VB} = 8.48 - 4.44 = 4.04 V
E_{CB} = 4.85 - 4.44 = 0.41 V

For PAA: E_g = 4.69 eV (calculated from the Tauc plot, Figure S64c)
E_{VB} = Width of the He I UPS spectra from the excitation energy (21.22 eV)
E_{VB} = 21.22 - (19.72 – 7.14) = 8.64 eV
$E_{CB} = E_{VB} - E_g$ = 3.95 eV
With respect to RHE:
E_{VB} = 8.64 - 4.44 = 4.20 V
E_{CB} = 4.97 - 4.44 = -0.49 V

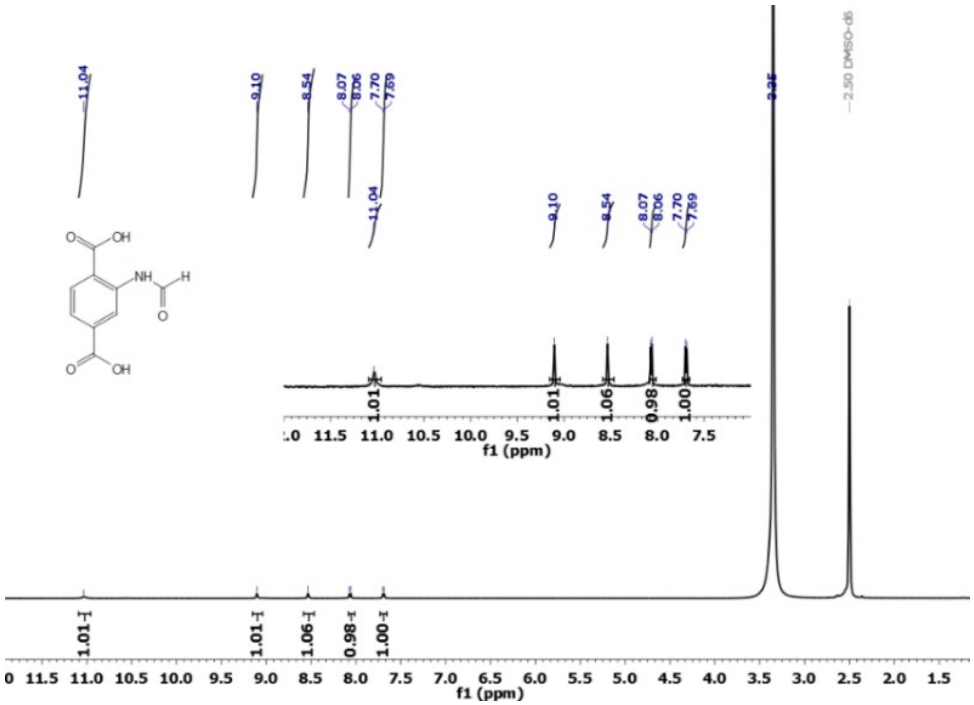

Figure S1. ^{1}H NMR spectrum of H_2BDC-NH-CHO ligand in DMSO-d_6.

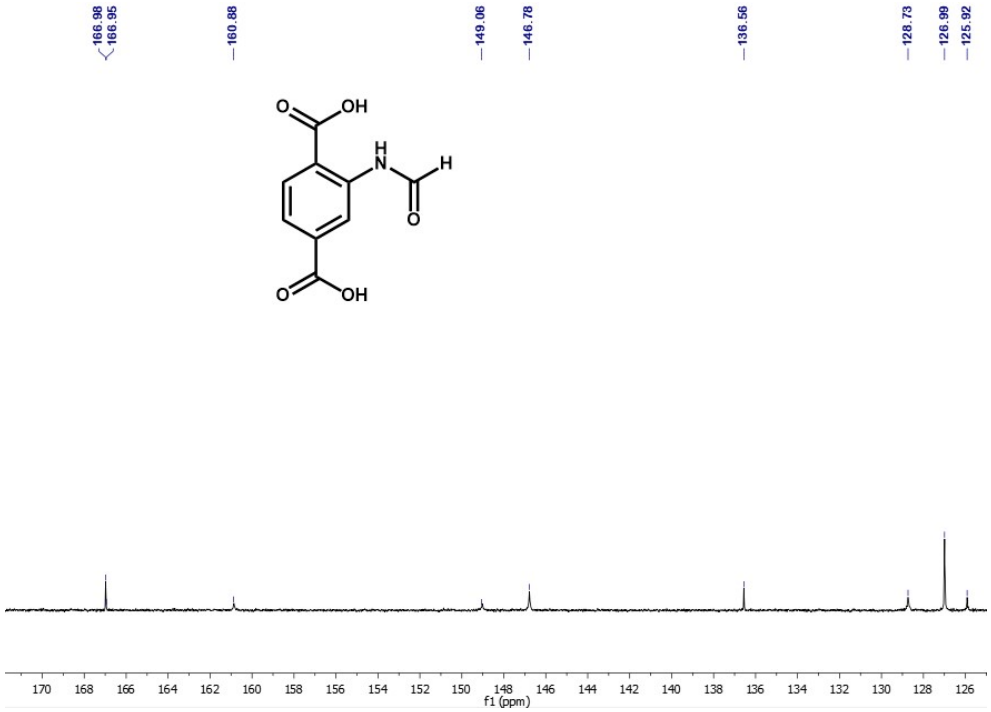

Figure S2. ^{13}C NMR spectrum of H_2BDC-NH-CHO ligand in DMSO-d_6.

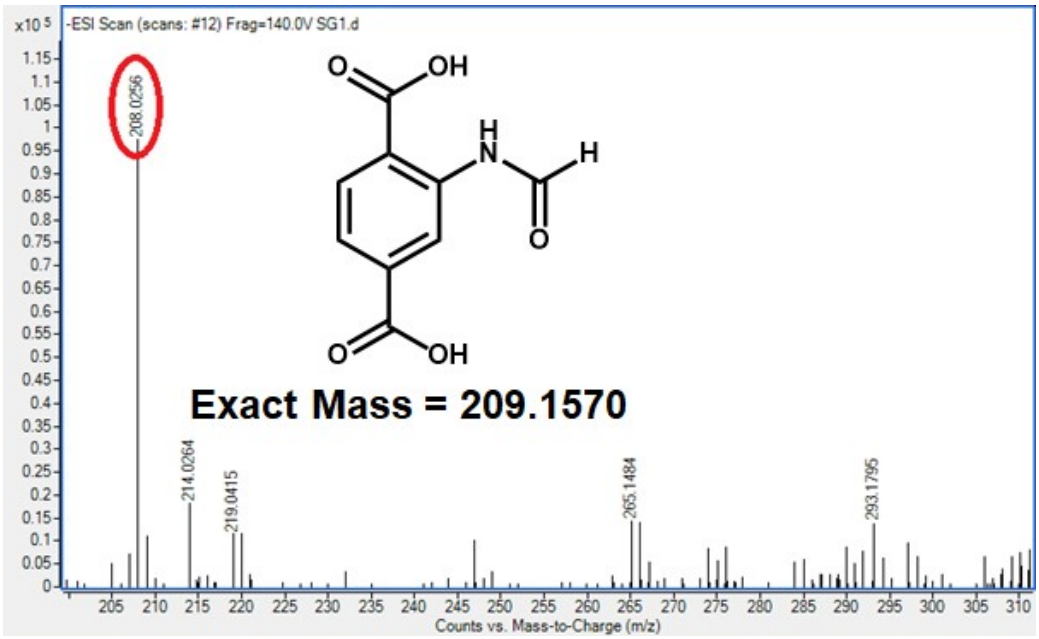

Figure S3. HR-MS spectrum of H_2BDC-NH-CHO ligand measured in methanol. The spectrum shows m/z peak at 208.0257, which corresponds to $(M-H)^-$ ion (M = mass of 2-formamidoterephthalic acid ligand).

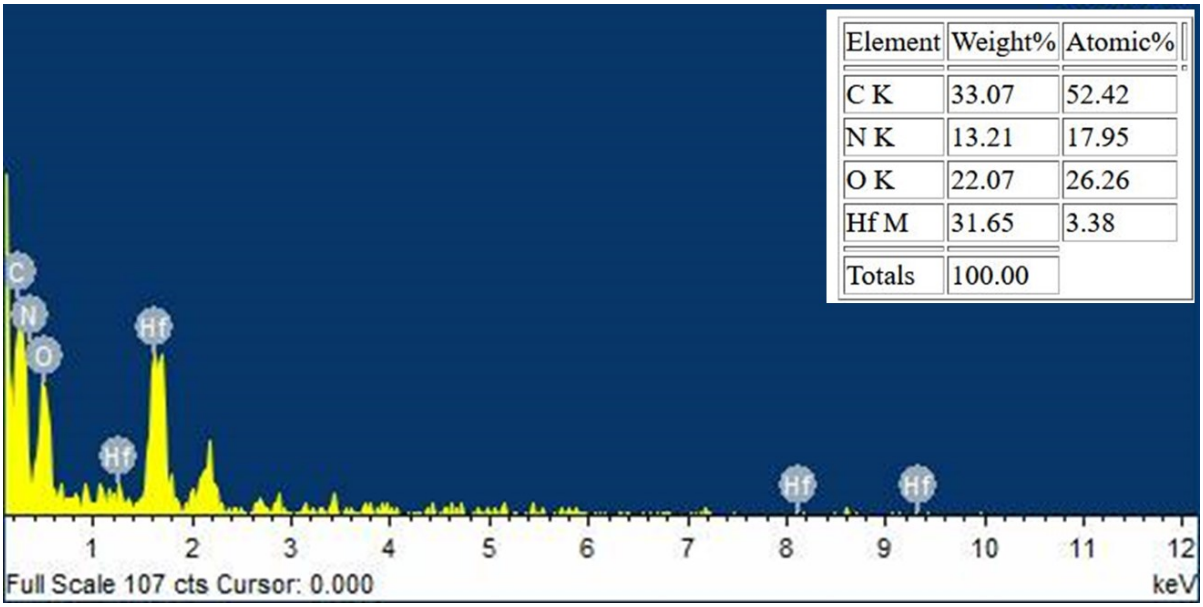

Figure S4. EDX spectrum of **1**.

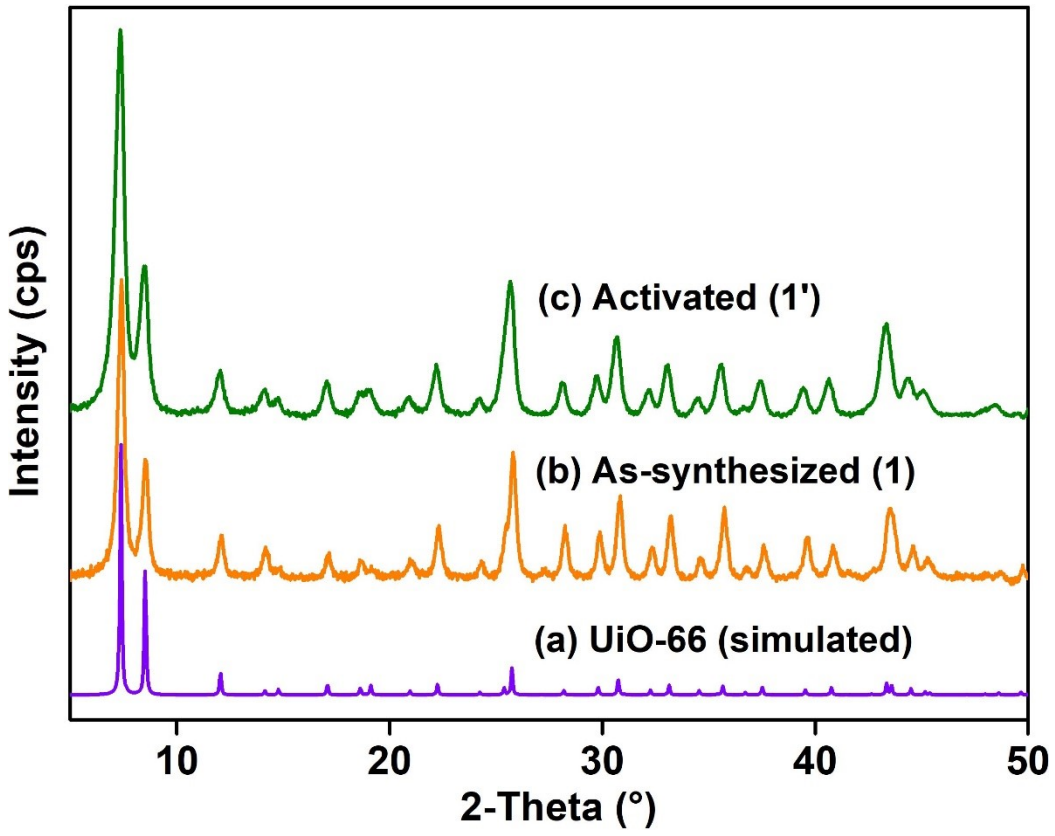

Figure S5. PXRD patterns of (a) simulated, (b) as-synthesized **1** and (c) activated **1′**.

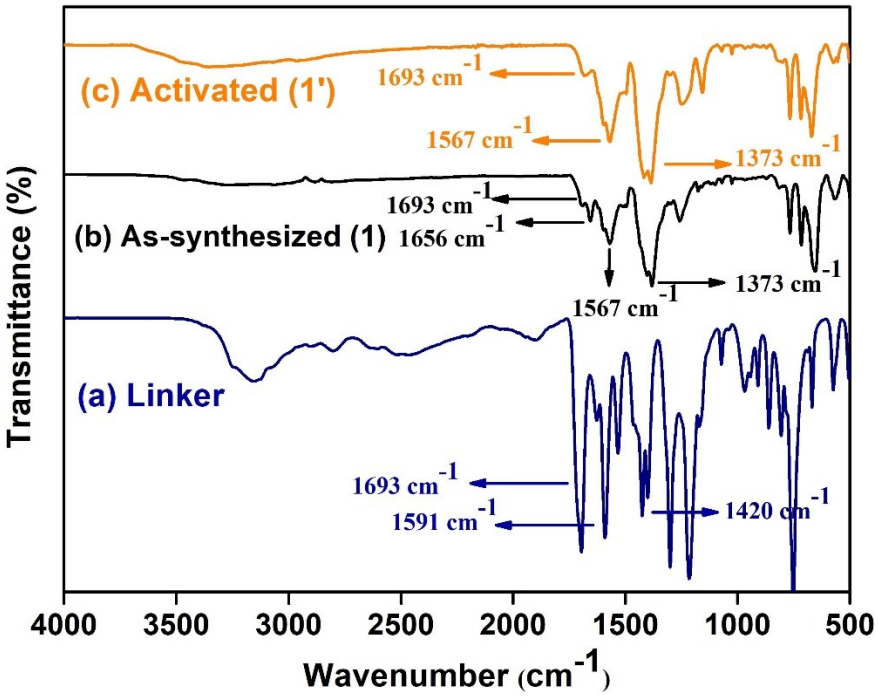

Figure S6. FT-IR spectra of (a) H_2BDC-NH-CHO linker, (b) **1** (as-synthesized) and (c) **1′** (activated).

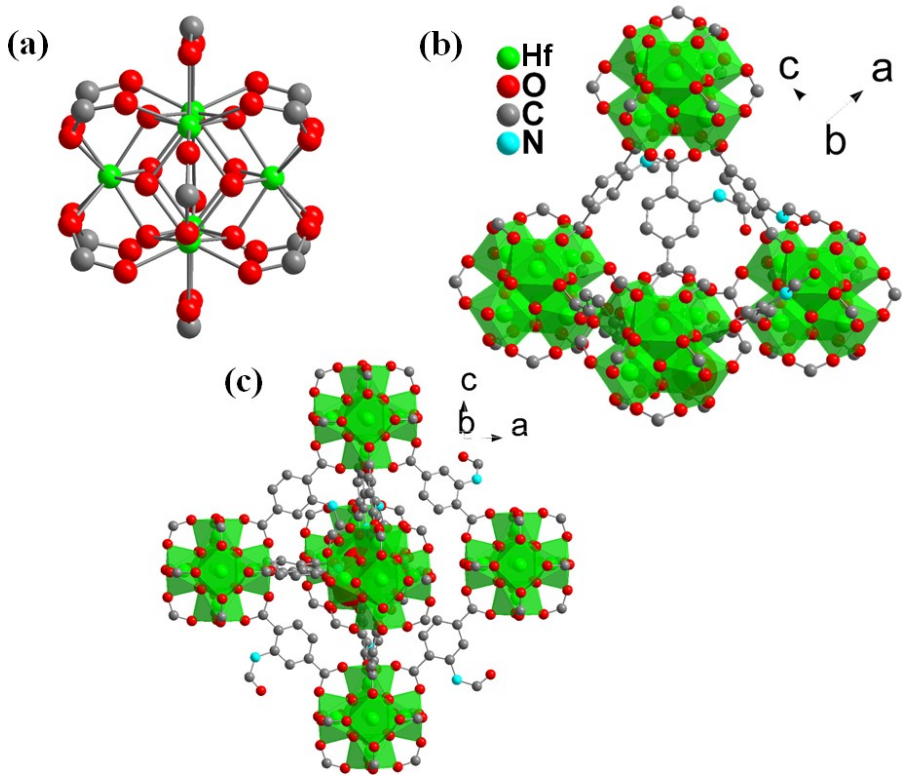

Figure S7. Structural drawings of the (a) hexa-nuclear $[Hf_6O_4(OH)_4]^{12+}$ cluster and larger (octahedral) and smaller (tetrahedral) voids present in the framework of compound **1**.

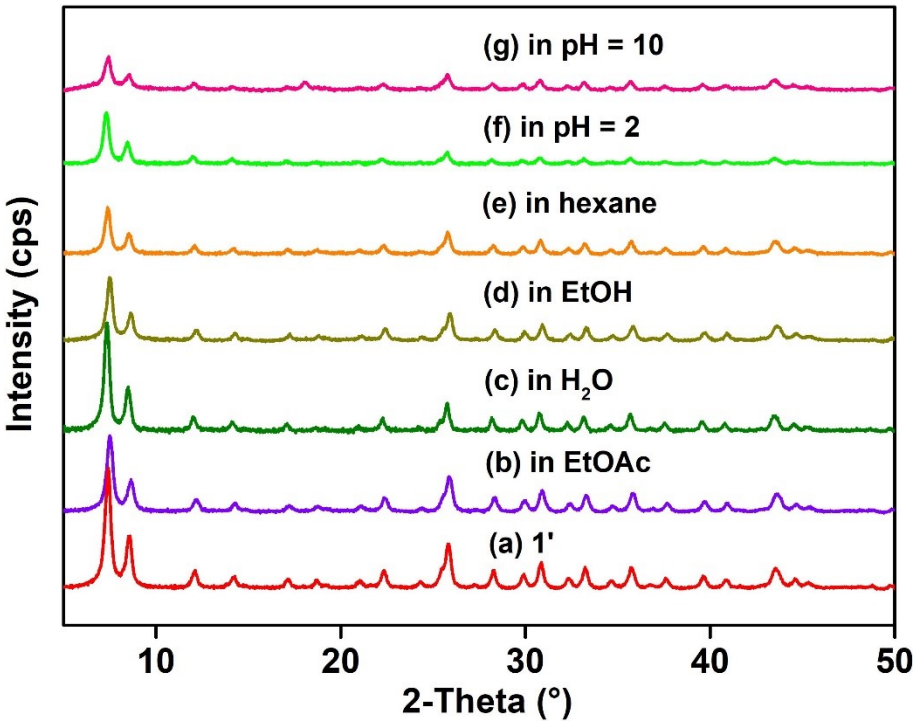

Figure S8. PXRD patterns of **1′** in different forms: (a) activated **1′**, after stirred in (b) EtOAc, (c) H_2O (d) EtOH, (e) hexane, (f) pH = 2 and (g) pH = 10.

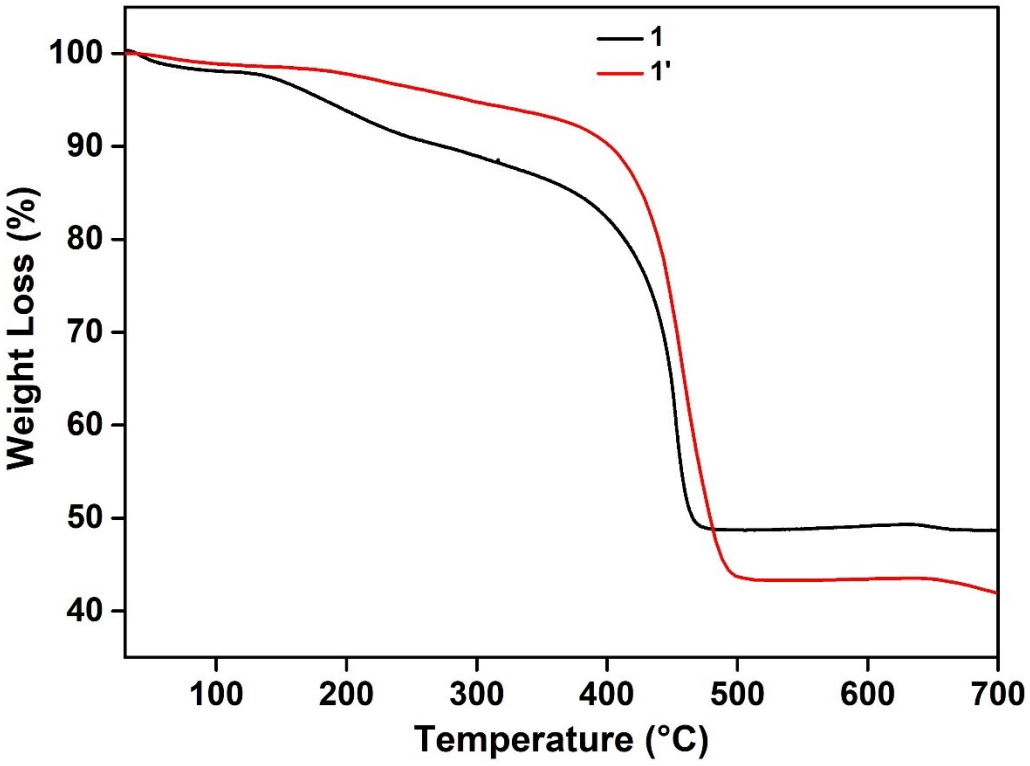

Figure S9. Thermogravimetric analysis curves of as-synthesized **1** (black) and thermally activated **1′** (red) recorded under O_2 atmosphere in the temperature range of 30-700 °C with a heating rate of 4 °C min^{-1}.

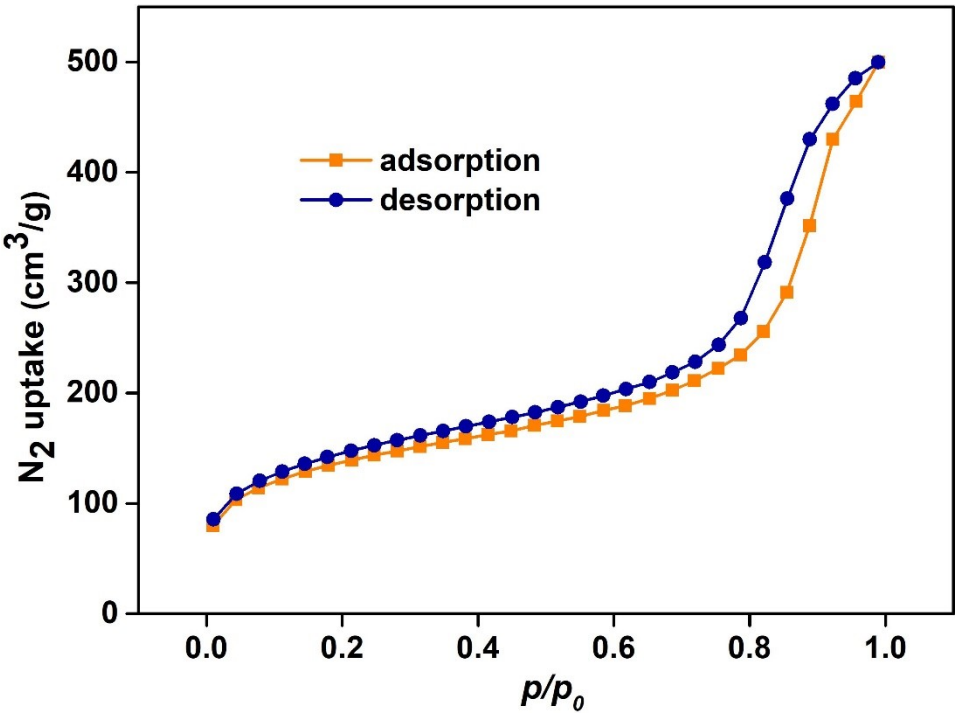

Figure S10. N_2 adsorption (yellow squares) and desorption (blue circles) isotherms of thermally activated **1′** recorded at –196 °C.

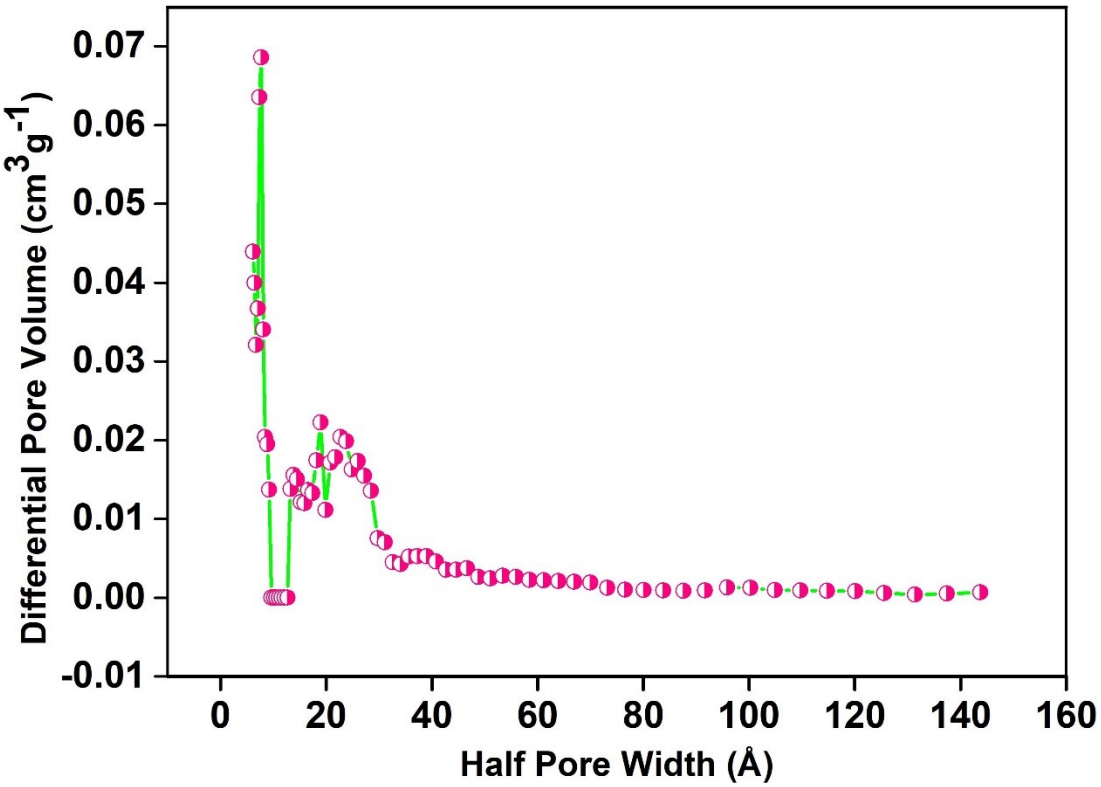

Figure S11. Density functional theory pore-size distribution of compound **1′** as determined from its N_2 adsorption isotherms at -196 °C.

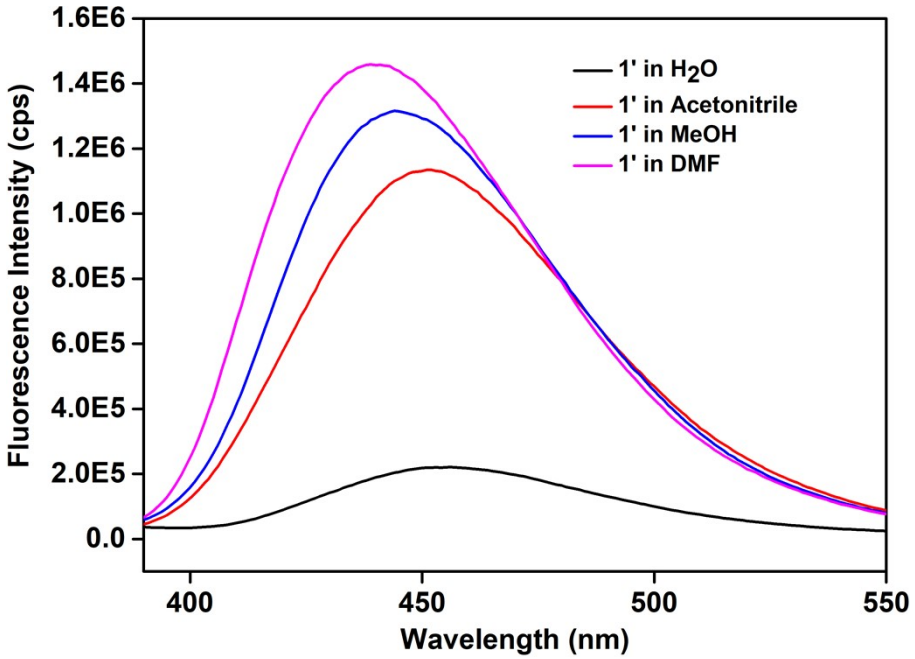

Figure S12. Fluorescence emission spectra of **1′** in various solvents (H_2O, acetonitrile, methanol and DMF).

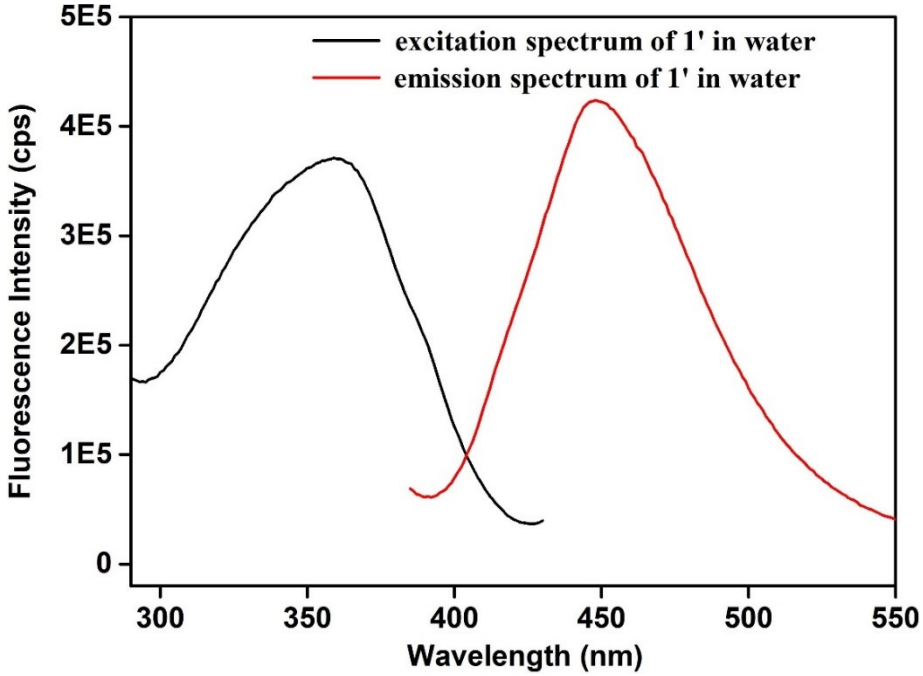

Figure S13. Excitation (black) and emission (red) spectra of **1′** in water.

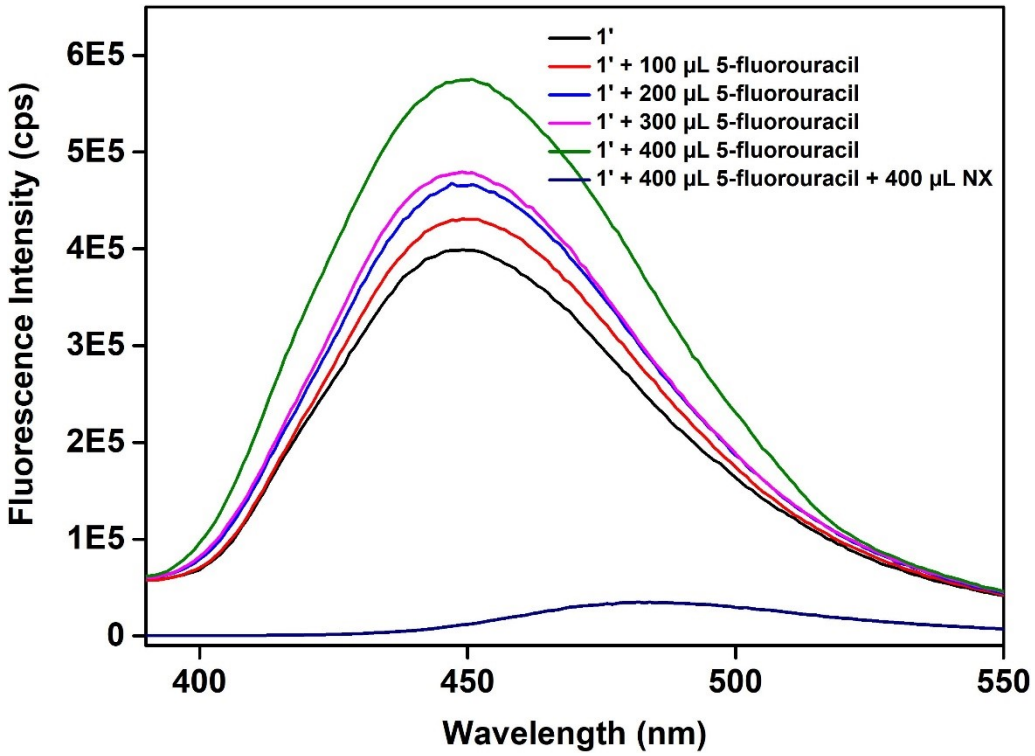

Figure S14. Quenching in fluorescence emission intensity of the suspension of **1′** in aqueous medium after addition of 400 µL of 10 mM aqueous NX solution in presence of 400 µL of 10 mM aqueous solution of 5-fluorouracil.

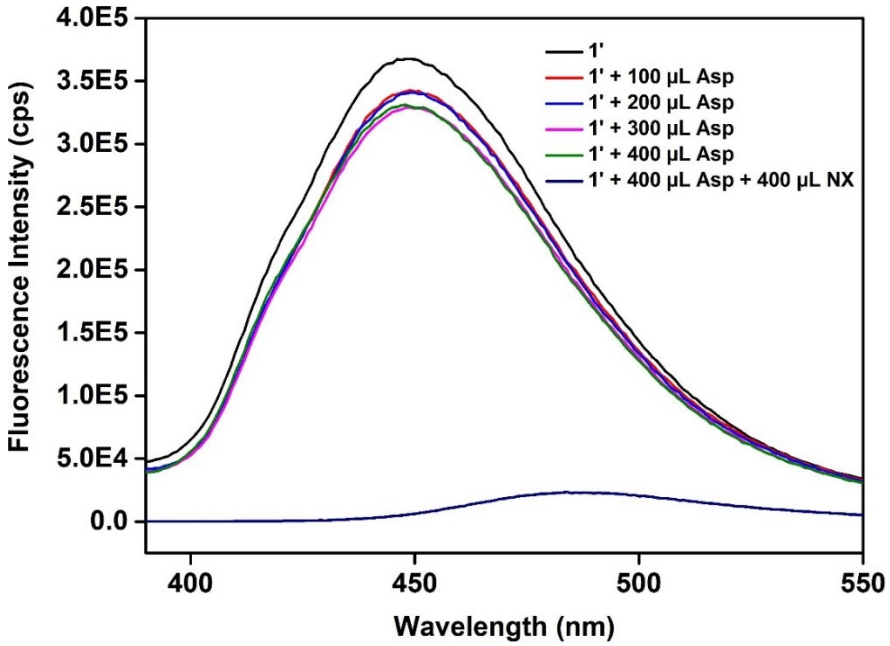

Figure S15. Quenching in fluorescence emission intensity of the suspension of **1′** in aqueous medium after addition of 400 µL of 10 mM aqueous NX solution in presence of 400 µL of 10 mM aqueous solution of aspartic acid (Asp).

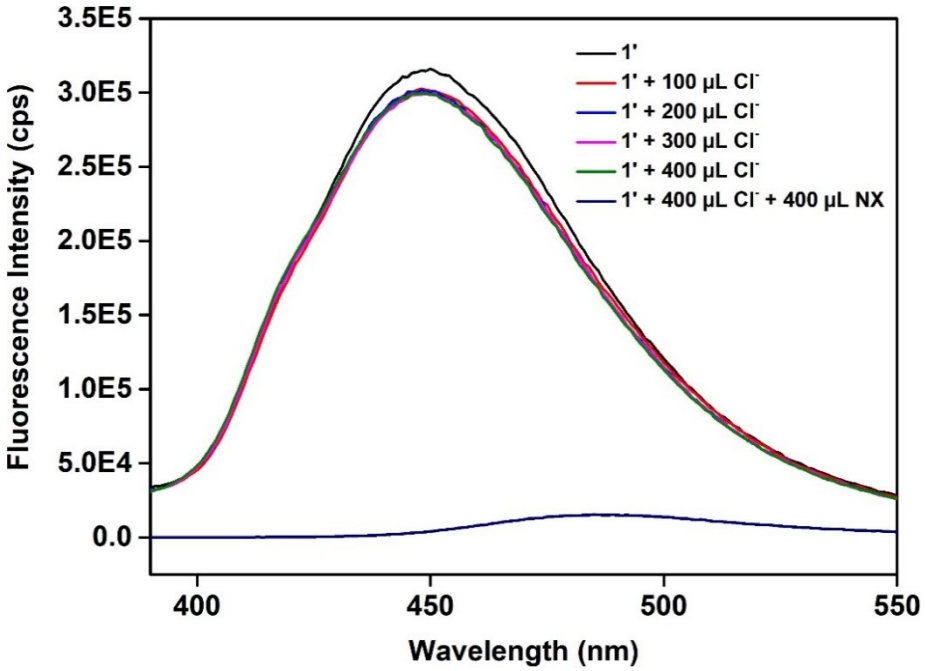

Figure S16. Quenching in fluorescence emission intensity of the suspension of **1′** in aqueous medium after addition of 400 µL of 10 mM aqueous NX solution in presence of 400 µL of 10 mM aqueous solution of Cl^-.

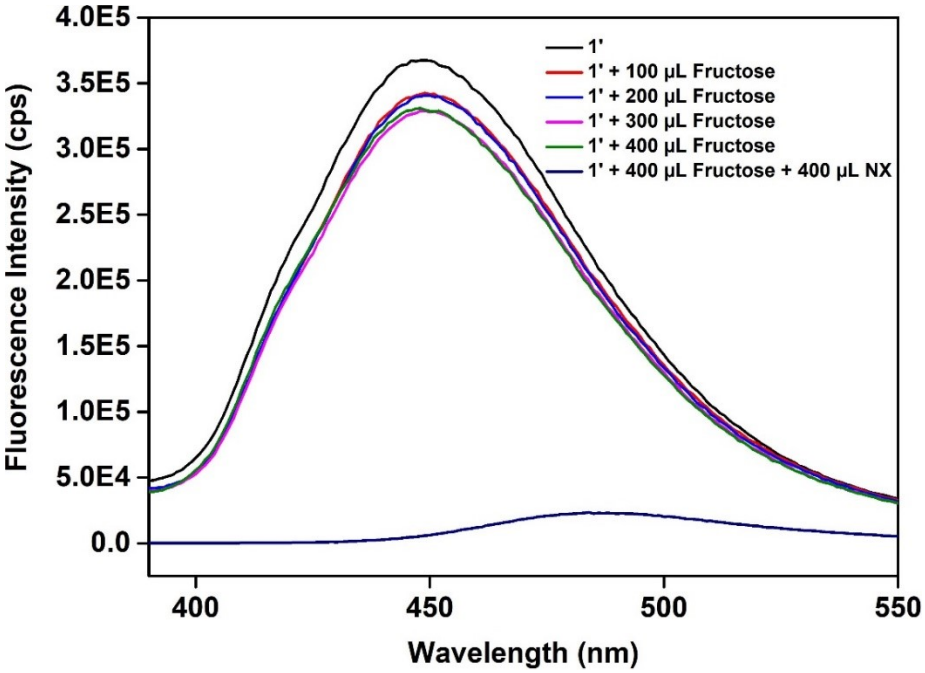

Figure S17. Quenching in fluorescence emission intensity of the suspension of **1′** in aqueous medium after addition of 400 µL of 10 mM aqueous NX solution in presence of 400 µL of 10 mM aqueous solution of fructose.

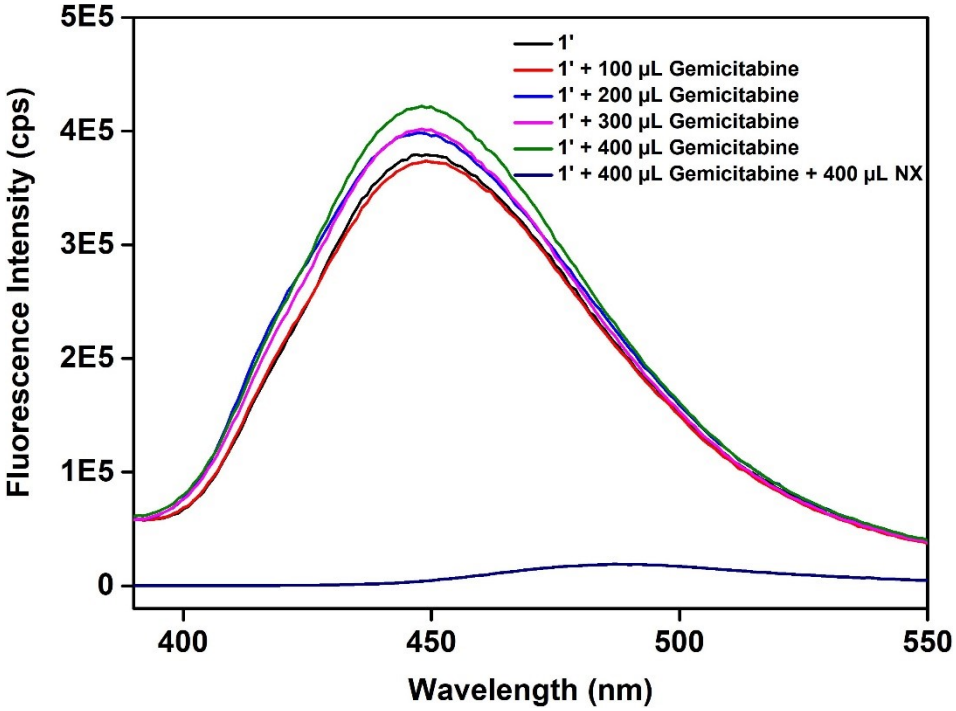

Figure S18. Quenching in fluorescence emission intensity of the suspension of **1′** in aqueous medium after addition of 400 µL of 10 mM aqueous NX solution in presence of 400 µL of 10 mM aqueous solution of gemicitabine.

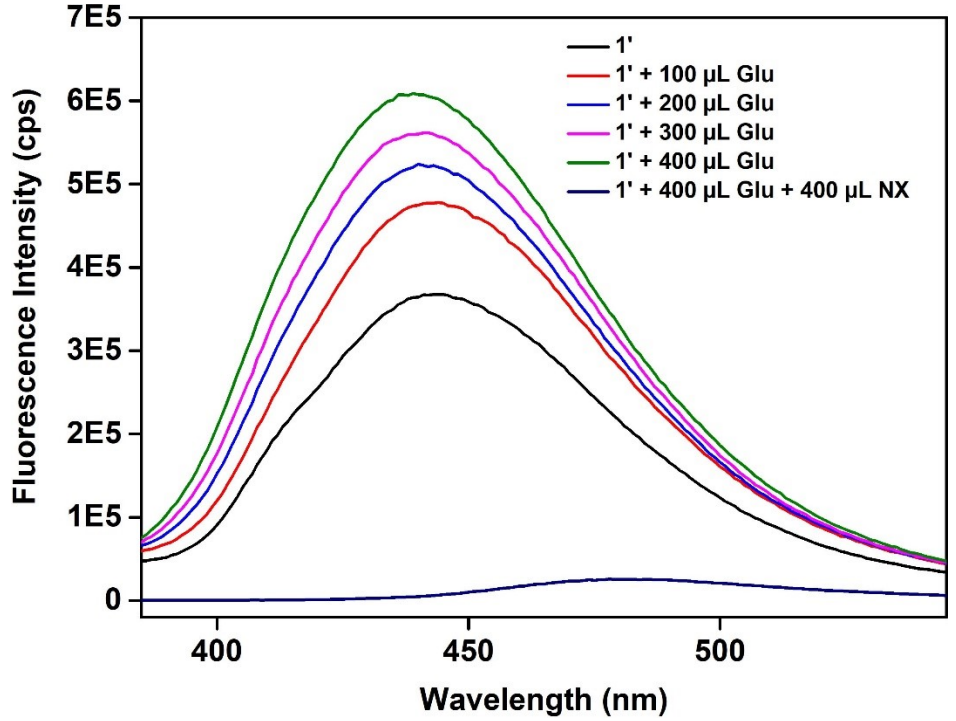

Figure S19. Quenching in fluorescence emission intensity of the suspension of **1′** in aqueous medium after addition of 400 µL of 10 mM aqueous NX solution in presence of 400 µL of 10 mM aqueous solution of glutamic acid (glu).

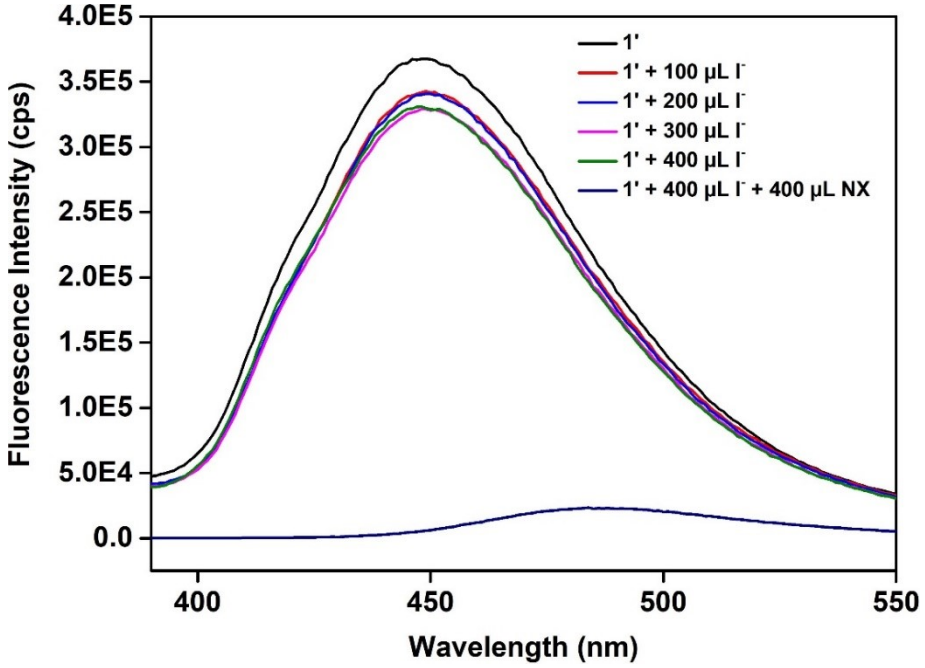

Figure S20. Quenching in fluorescence emission intensity of the suspension of **1′** in aqueous medium after addition of 400 µL of 10 mM aqueous NX solution in presence of 400 µL of 10 mM aqueous solution of I^-.

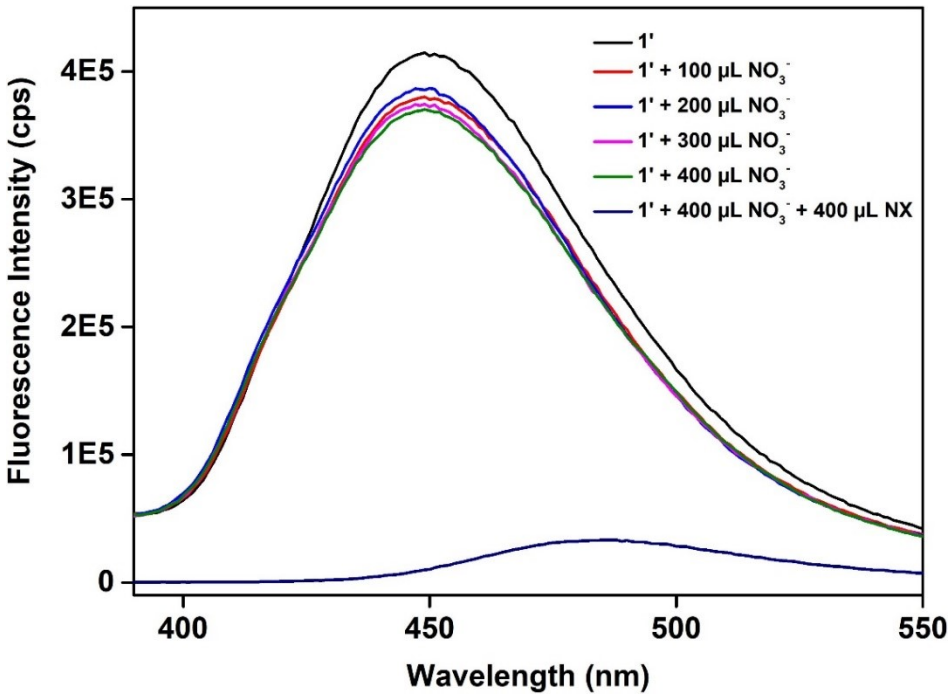

Figure S21. Quenching in fluorescence emission intensity of the suspension of **1′** in aqueous medium after addition of 400 µL of 10 mM aqueous NX solution in presence of 400 µL of 10 mM aqueous solution of NO_3^-.

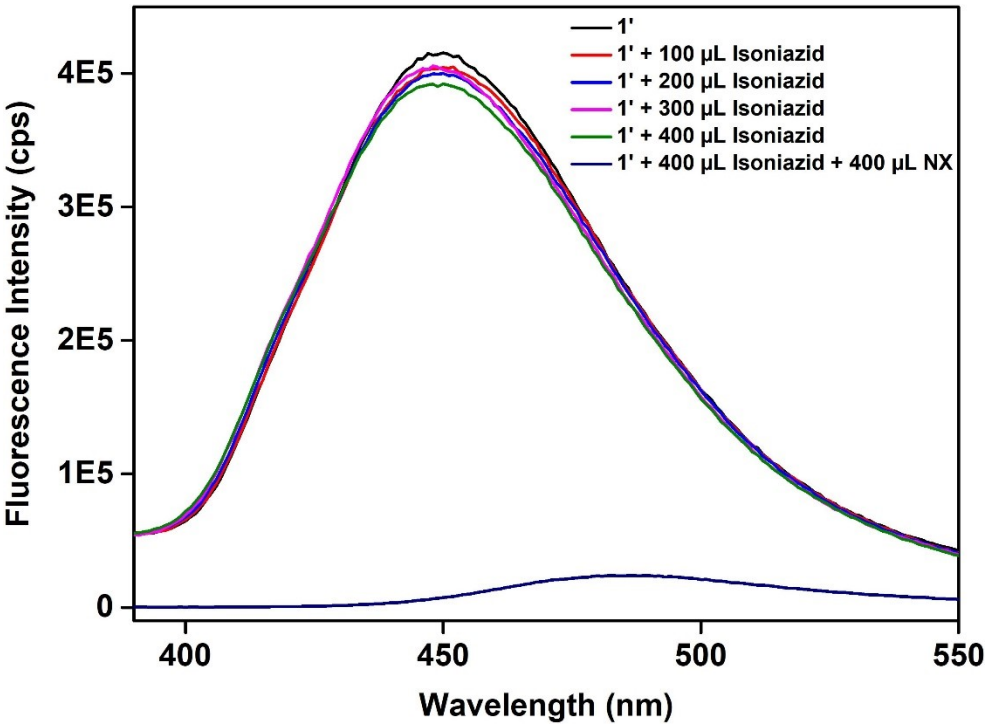

Figure S22. Quenching in fluorescence emission intensity of the suspension of **1′** in aqueous medium after addition of 400 µL of 10 mM aqueous NX solution in presence of 400 µL of 10 mM aqueous solution of isonizide.

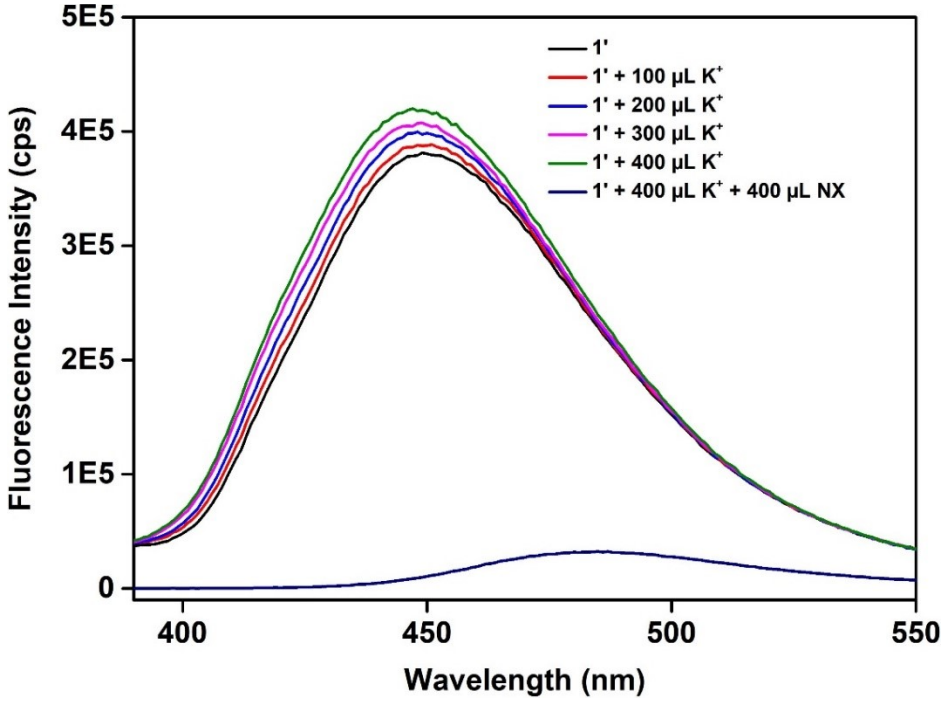

Figure S23. Quenching in fluorescence emission intensity of the suspension of **1′** in aqueous medium after addition of 400 µL of 10 mM aqueous NX solution in presence of 400 µL of 10 mM aqueous solution of K^+.

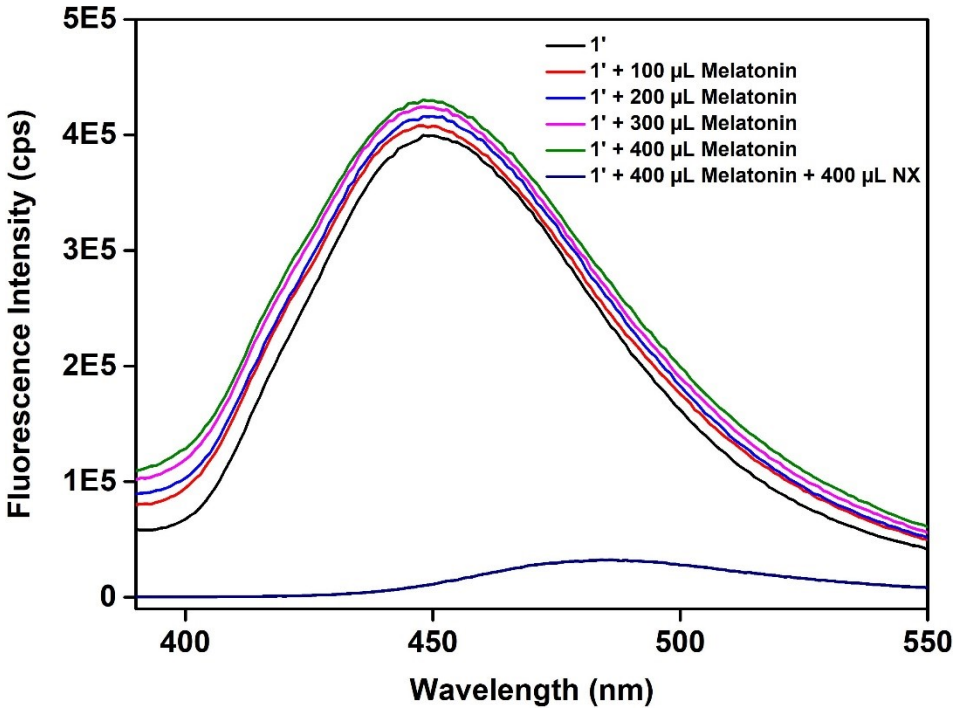

Figure S24. Quenching in fluorescence emission intensity of the suspension of **1′** in aqueous medium after addition of 400 µL of 10 mM aqueous NX solution in presence of 400 µL of 10 mM aqueous solution of melatonin.

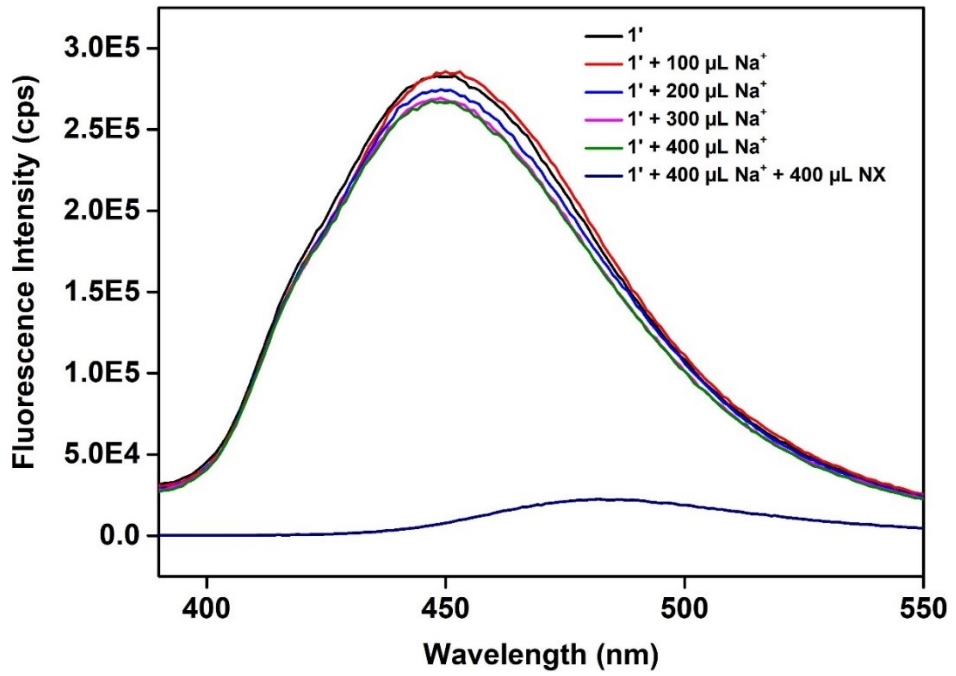

Figure S25. Quenching in fluorescence emission intensity of the suspension of **1′** in aqueous medium after addition of 400 µL of 10 mM aqueous NX solution in presence of 400 µL of 10 mM aqueous solution of Na^+.

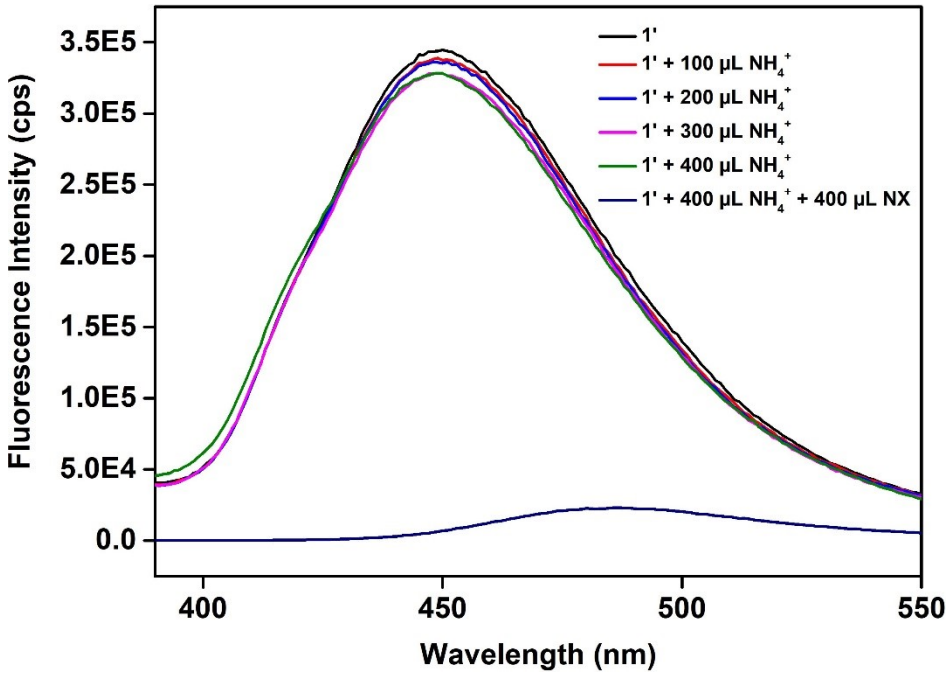

Figure S26. Quenching in fluorescence emission intensity of the suspension of **1′** in aqueous medium after addition of 400 µL of 10 mM aqueous NX solution in presence of 400 µL of 10 mM aqueous solution of NH_4^+.

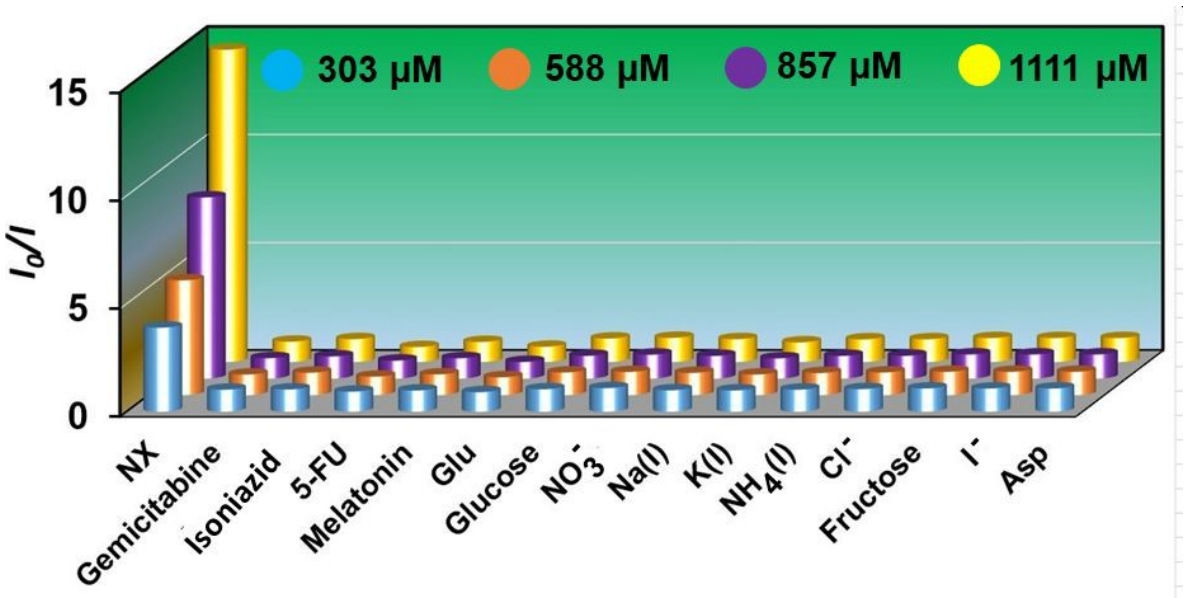

Figure S27. Stern-Volmers plot for the decrease in luminescence intensities of **1′** with gradual addition of various analytes in case of NX sensing.

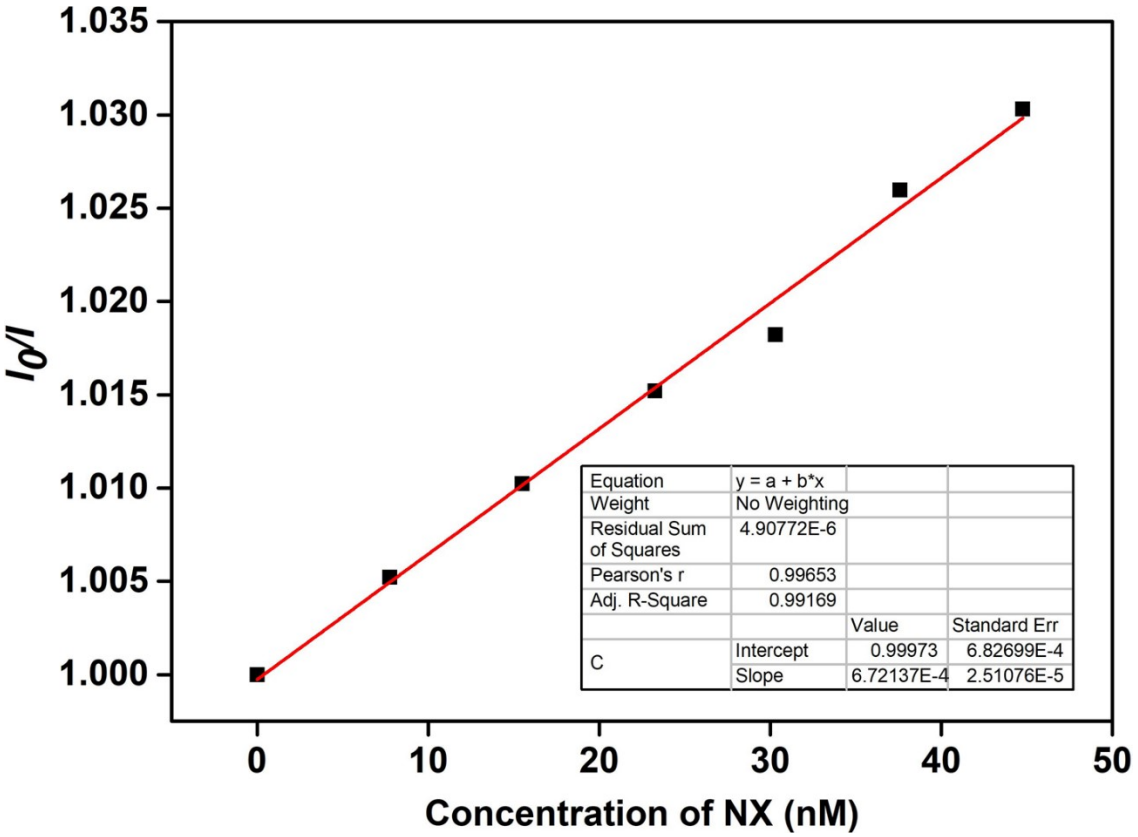

Figure S28. Stern-Volmer plot for the fluorescence emission quenching of **1′** in presence of NX.

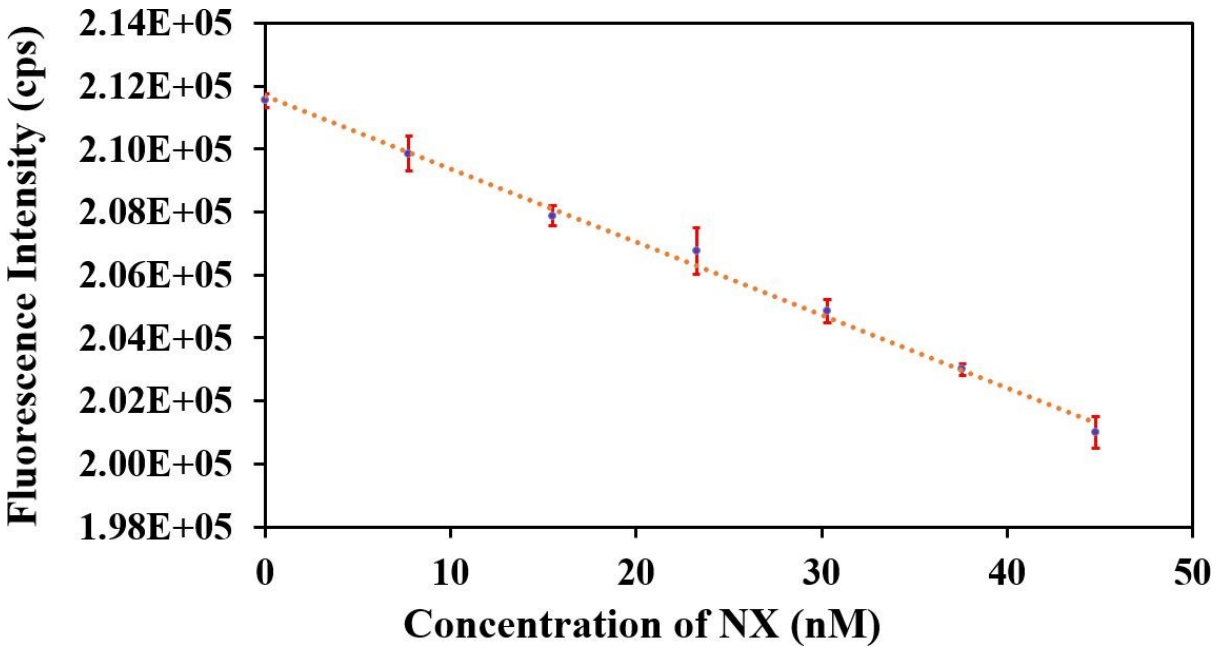

Figure S29. Change in the fluorescence emission intensity of **1′** in H_2O as a function of concentration of NX (the error bars shown in the plot represent the standard deviations of three separate measurements).

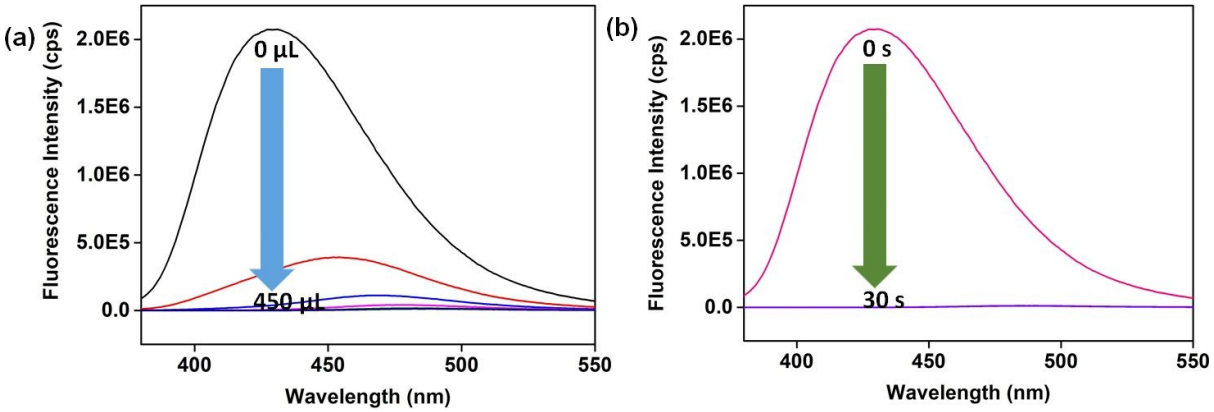

Figure S30. Change in fluorescence intensity of **1′** (a) with increasing volume of NX and (b) as a function of time in HEPES buffer medium.

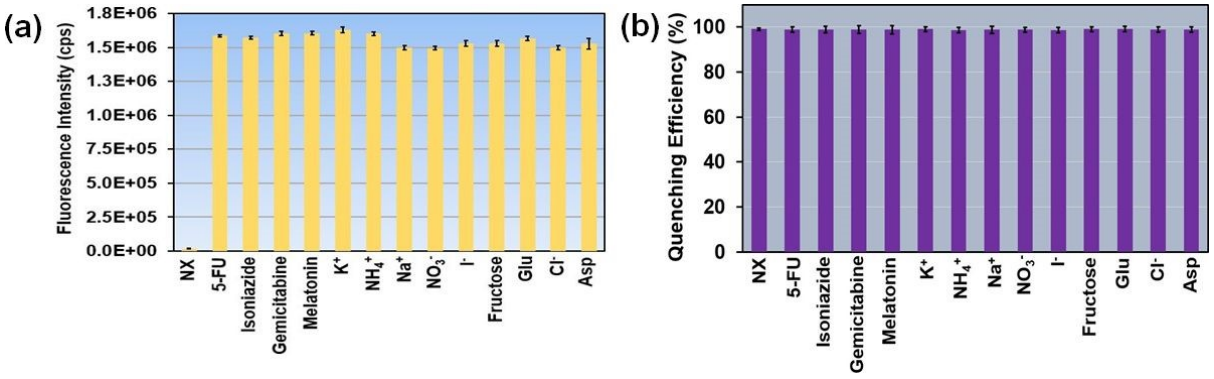

Figure S31. (a) Change in fluorescence intensity of **1′** in presence of various competitive analytes and (b) quenching efficiency of **1′** in presence of competitive analytes in HEPES buffer medium.

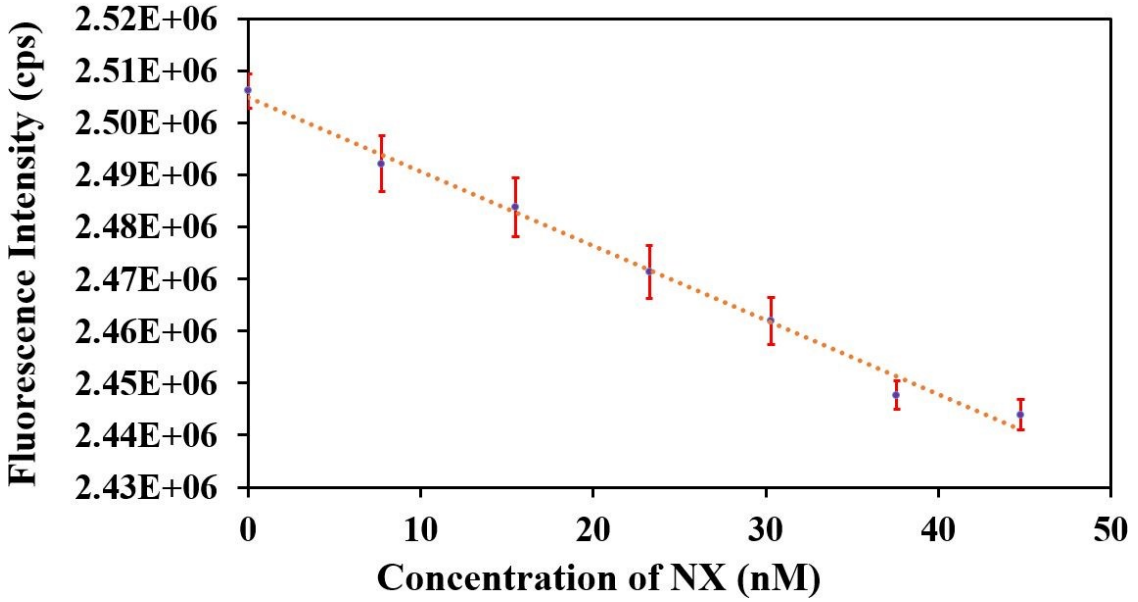

Figure S32. Change in the fluorescence emission intensity of **1′** in HEPES as a function of concentration of NX (the error bars shown in the plot represent the standard deviations of three separate measurements).

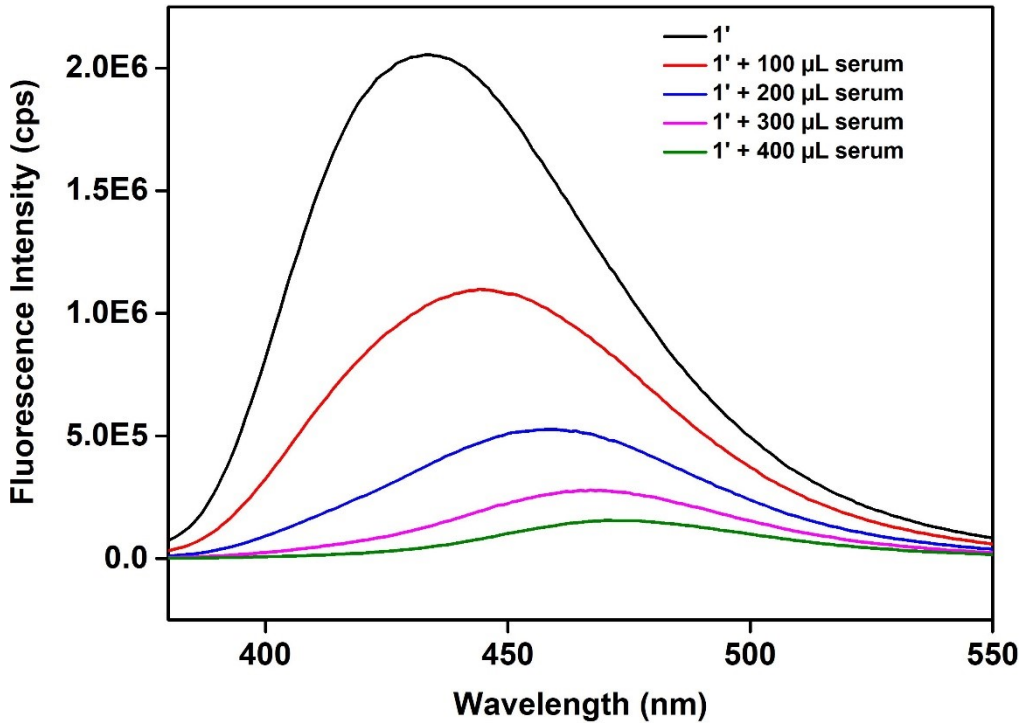

Figure S33. Turn-off in fluorescence emission intensity of the suspension of **1′** in HEPES buffer medium after addition of 5 mM of different volumes of NX-spiked serum solution.

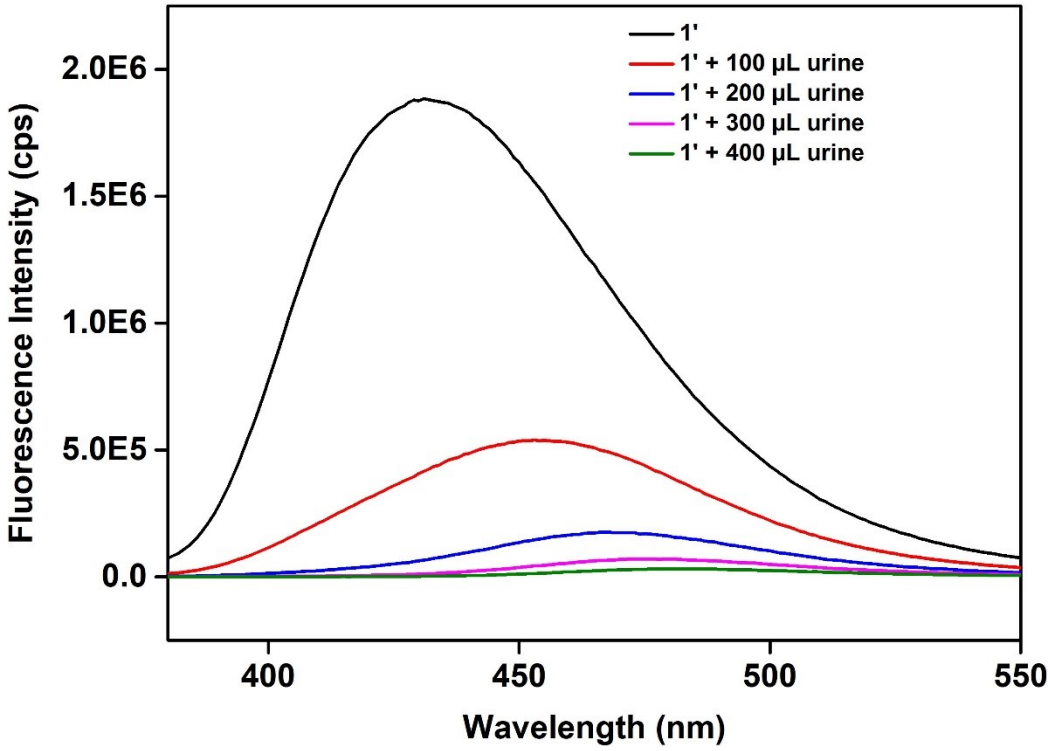

Figure S34. Turn-off in fluorescence emission intensity of the suspension of **1′** in HEPES buffer medium after addition of 5 mM different volumes of NX-spiked urine solution.

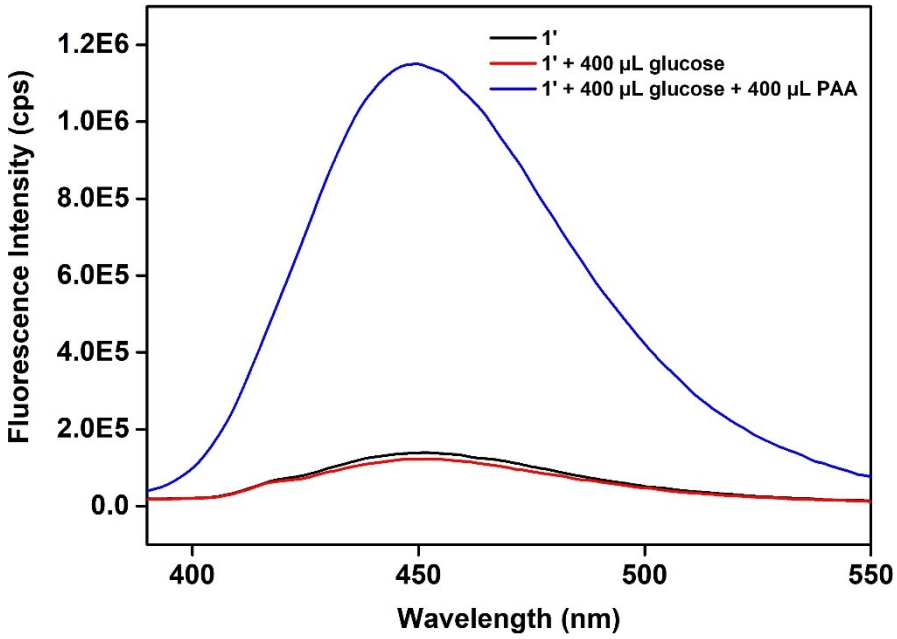

Figure S35. Increment in fluorescence emission intensity of the suspension of **1′** in H_2O after addition of 400 µL of 5 mM PAA solution in presence of 400 µL of 5 mM solution of glucose.

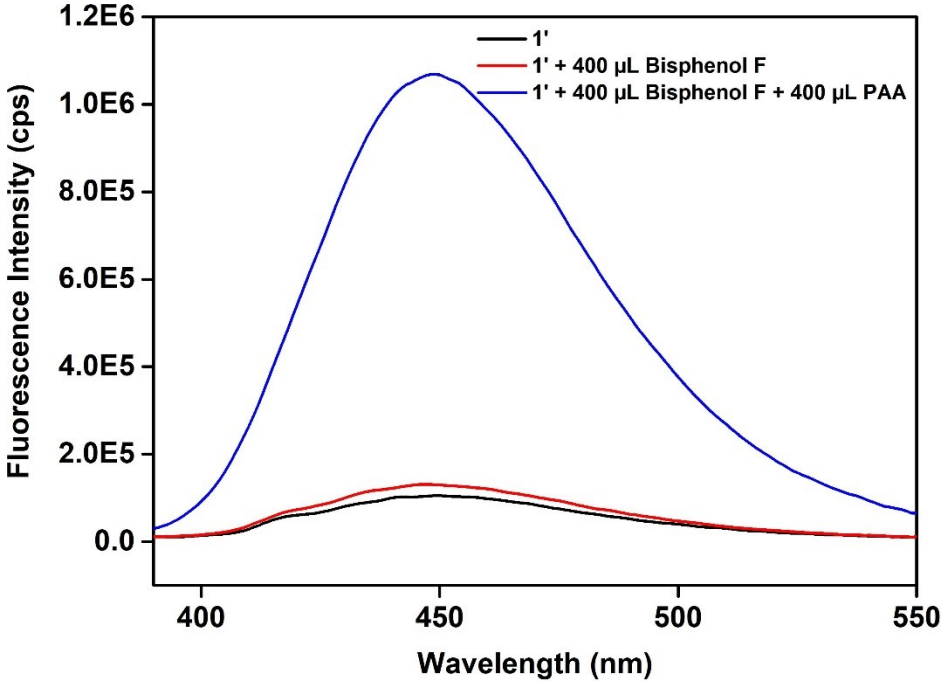

Figure S36. Increment in fluorescence emission intensity of the suspension of **1′** in H_2O after addition of 400 µL of 5 mM PAA solution in presence of 400 µL of 5 mM solution of bisphenol F.

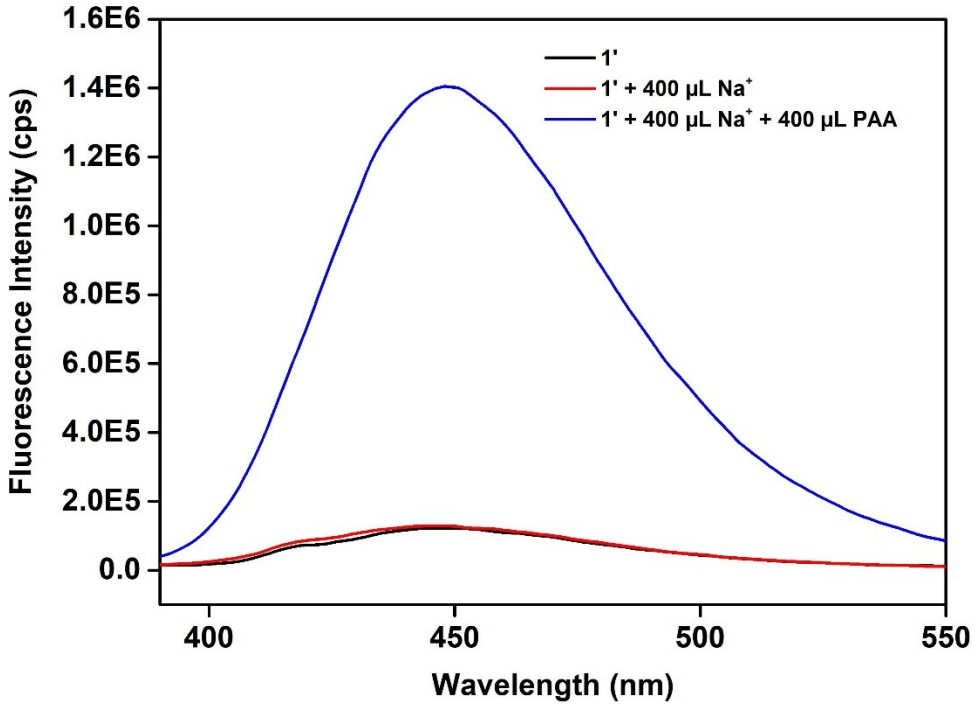

Figure S37. Increment in fluorescence emission intensity of the suspension of **1′** in H_2O after addition of 400 µL of 5 mM PAA solution in presence of 400 µL of 5 mM solution of Na^+.

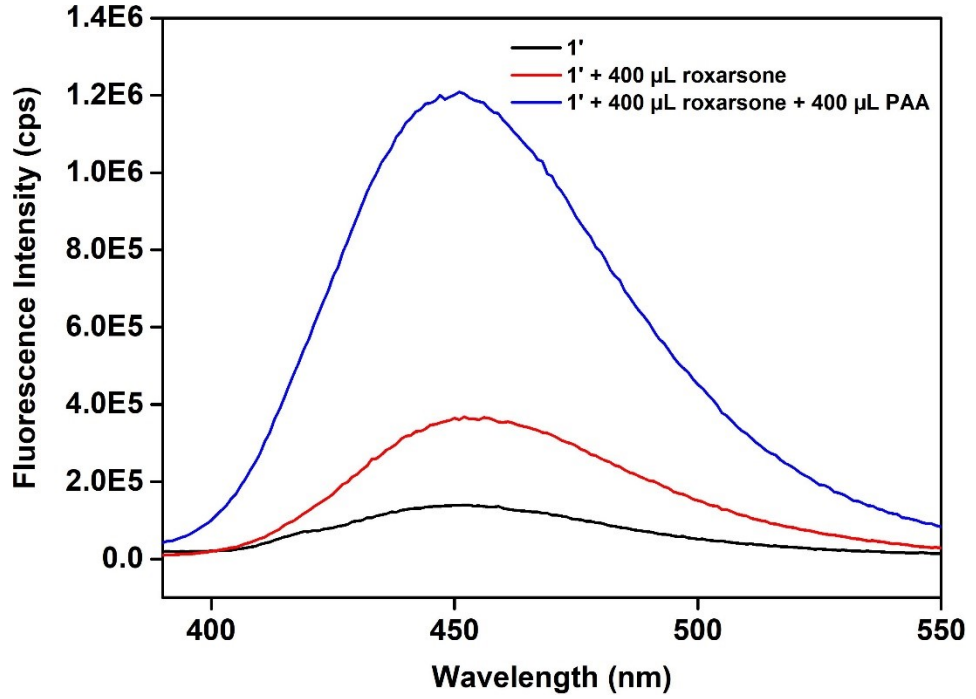

Figure S38. Increment in fluorescence emission intensity of the suspension of **1′** in H_2O after addition of 400 µL of 5 mM PAA solution in presence of 400 µL of 5 mM solution of roxarsone.

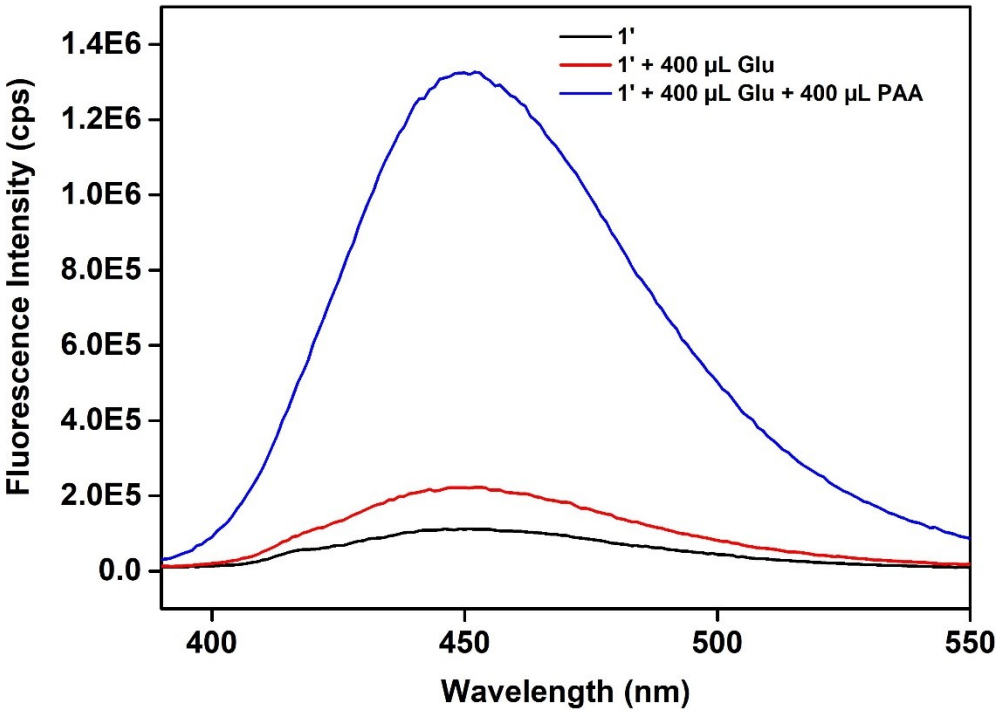

Figure S39. Increment in fluorescence emission intensity of the suspension of **1′** in H_2O after addition of 400 µL of 5 mM PAA solution in presence of 400 µL of 5 mM solution of glutamic acid.

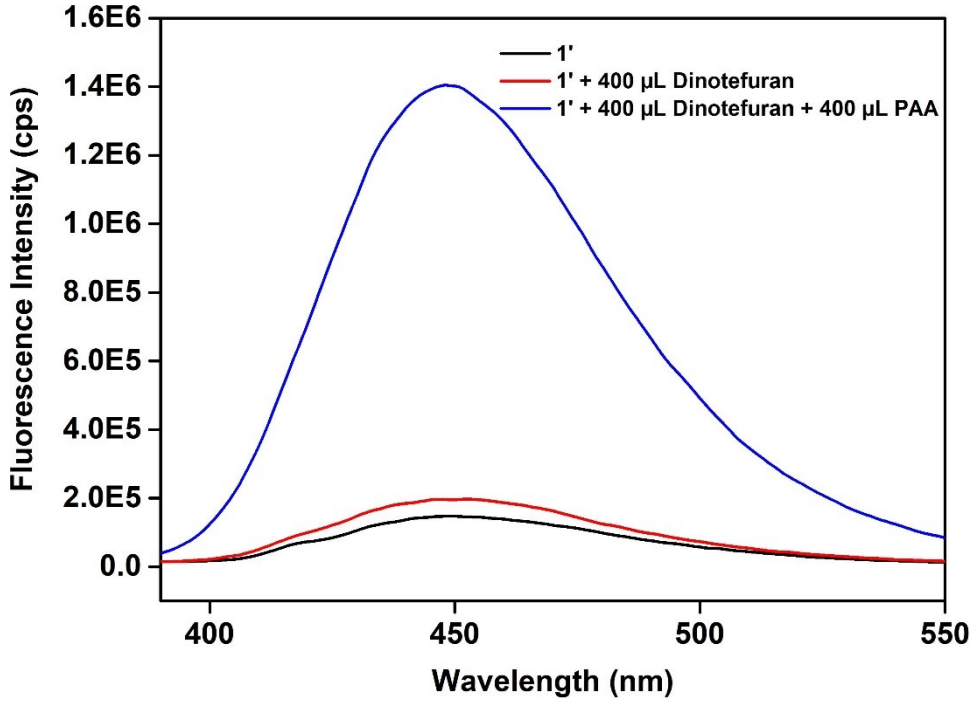

Figure S40. Increment in fluorescence emission intensity of the suspension of **1′** in H_2O after addition of 400 µL of 5 mM PAA solution in presence of 400 µL of 5 mM solution of dinotefuran.

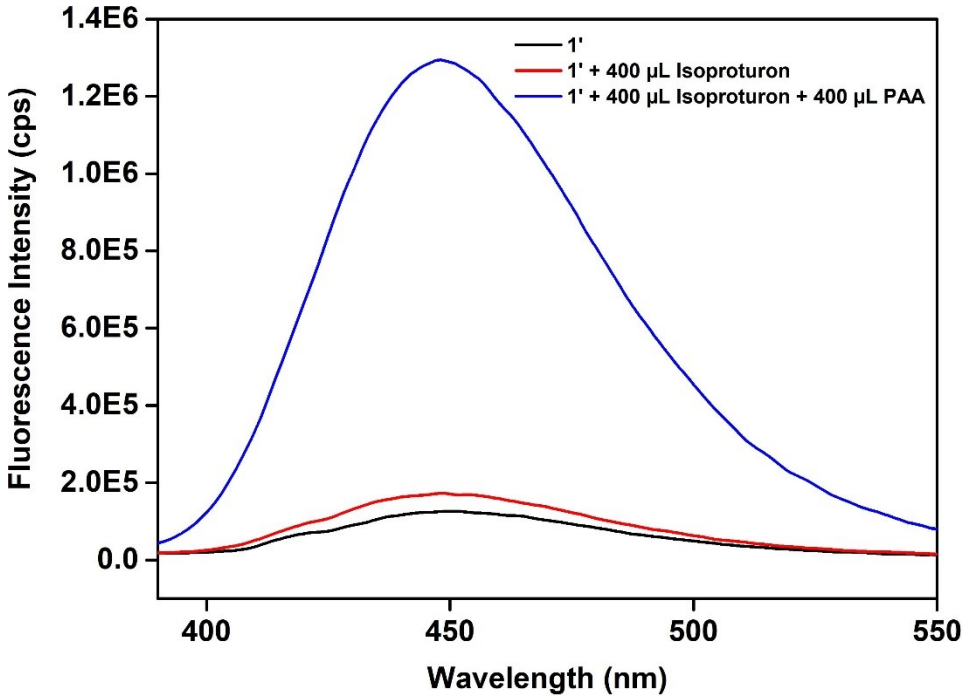

Figure S41. Increment in fluorescence emission intensity of the suspension of **1′** in H_2O after addition of 400 µL of 5 mM PAA solution in presence of 400 µL of 5 mM solution of isoproturon.

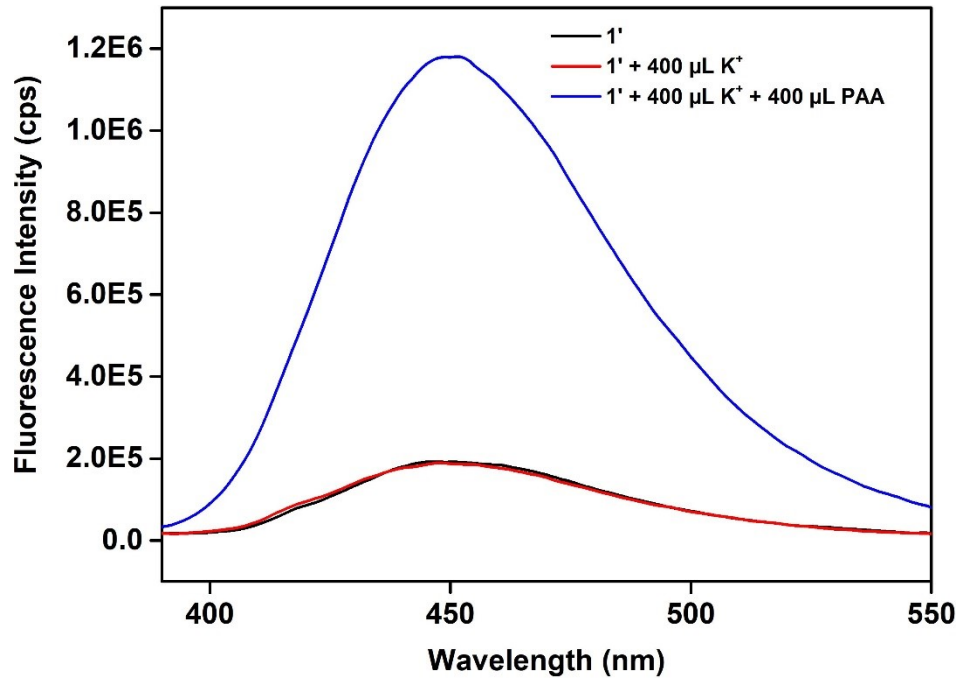

Figure S42. Increment in fluorescence emission intensity of the suspension of **1′** in H_2O after addition of 400 µL of 5 mM PAA solution in presence of 400 µL of 5 mM solution of K^+.

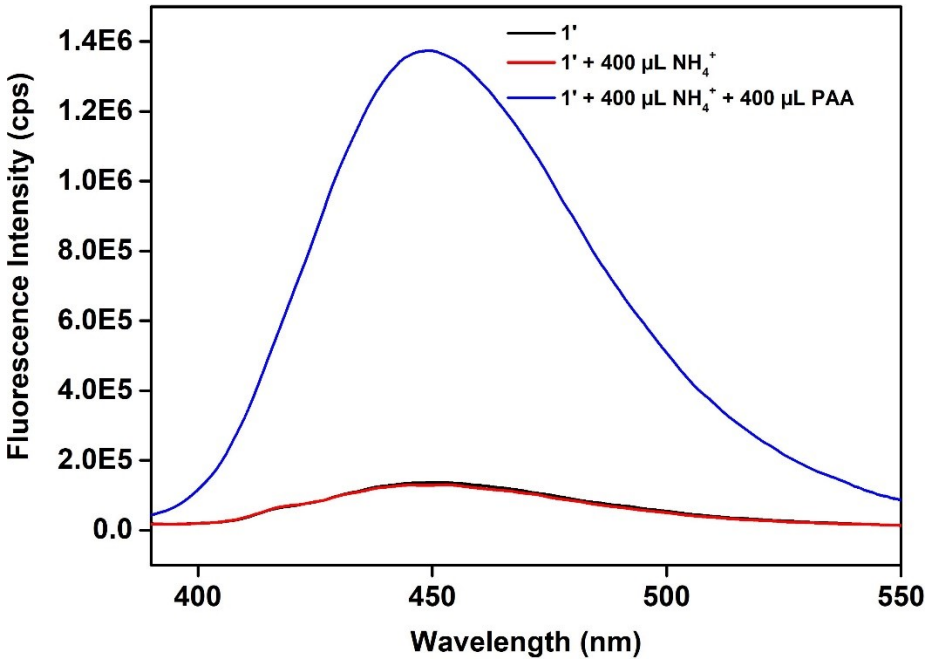

Figure S43. Increment in fluorescence emission intensity of the suspension of **1′** in H_2O after addition of 400 µL of 5 mM PAA solution in presence of 400 µL of 5 mM solution of NH_4^+.

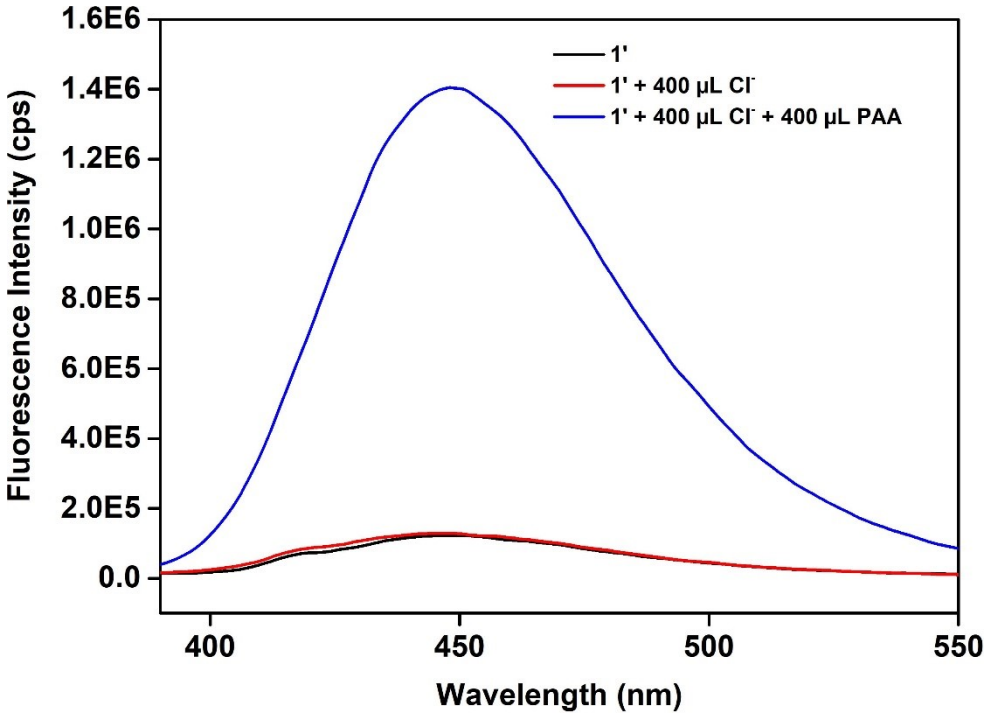

Figure S44. Increment in fluorescence emission intensity of the suspension of **1′** in H_2O after addition of 400 µL of 5 mM PAA solution in presence of 400 µL of 5 mM solution of Cl^-.

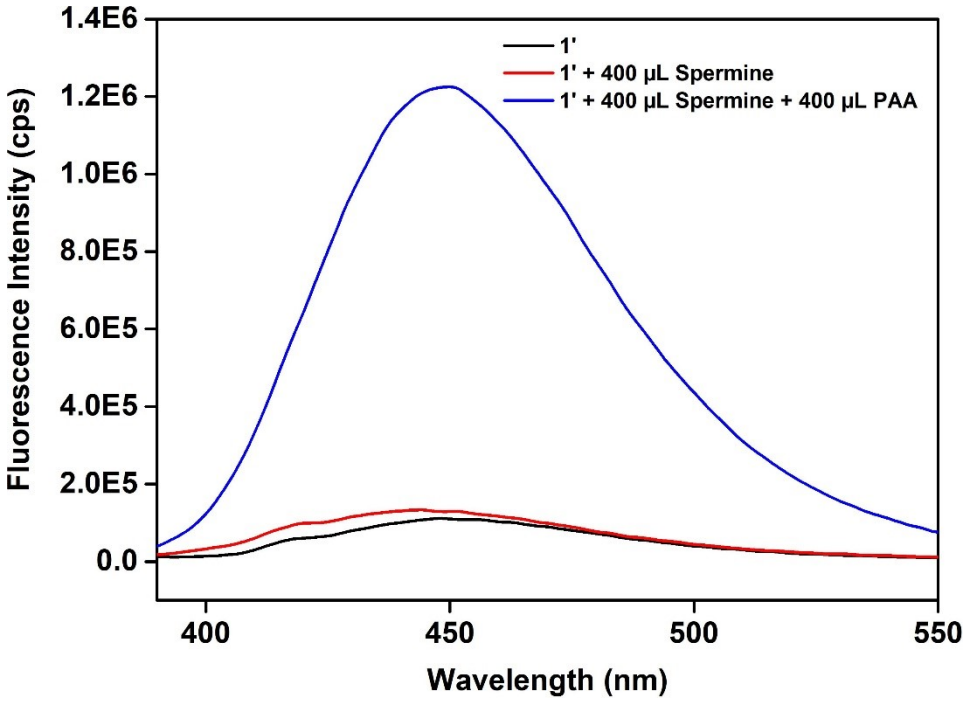

Figure S45. Increment in fluorescence emission intensity of the suspension of **1′** in H_2O after addition of 400 µL of 5 mM PAA solution in presence of 400 µL of 5 mM solution of spermine.

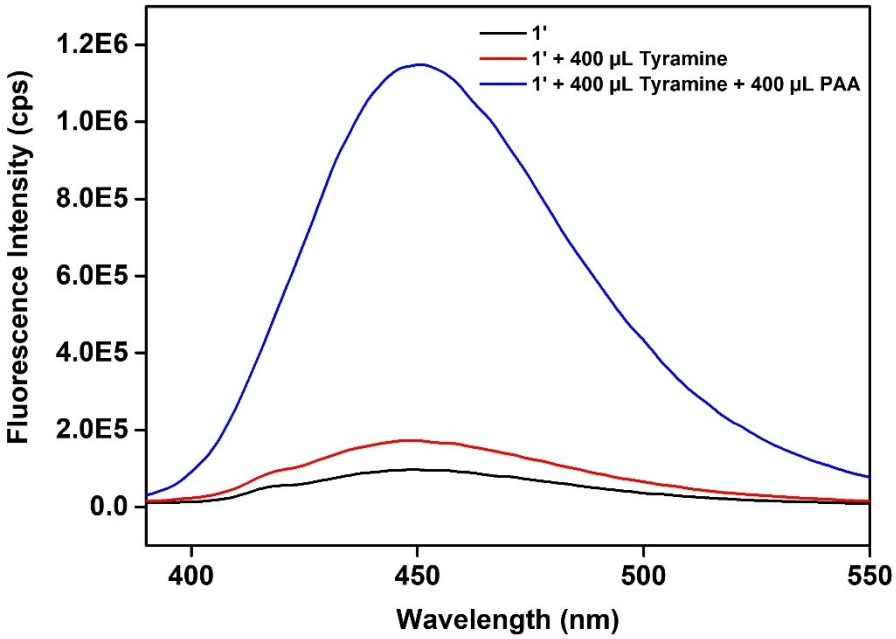

Figure S46. Increment in fluorescence emission intensity of the suspension of **1′** in H_2O after addition of 400 µL of 5 mM PAA solution in presence of 400 µL of 5 mM solution of tyramine.

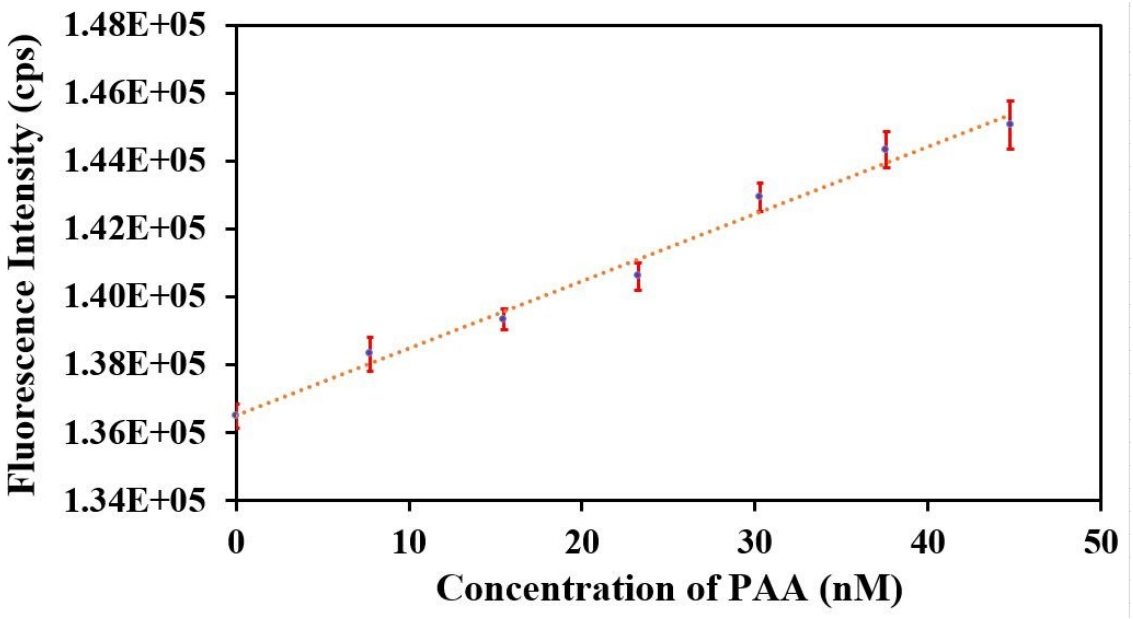

Figure S47. Change in the fluorescence emission intensity of **1′** in water as a function of concentration of PAA (the error bars shown in the plot represent the standard deviations of three separate measurements).

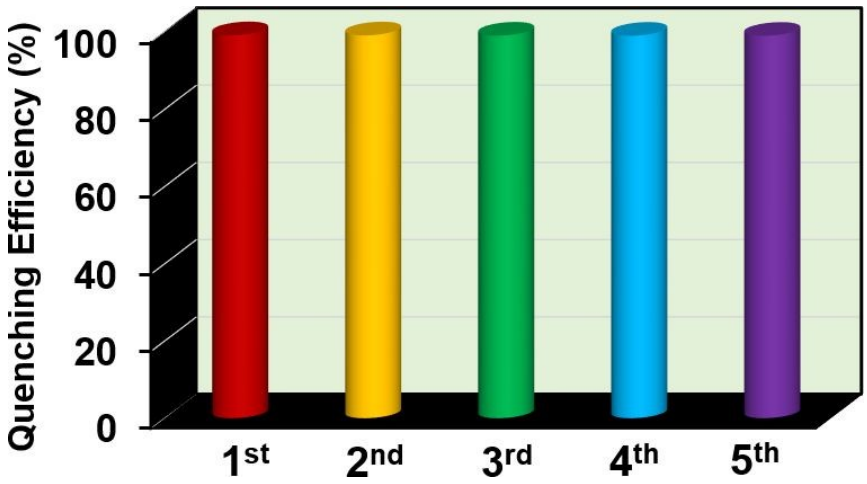

Figure S48. Reusability of **1′** for the sensing of NX in aqueous medium.

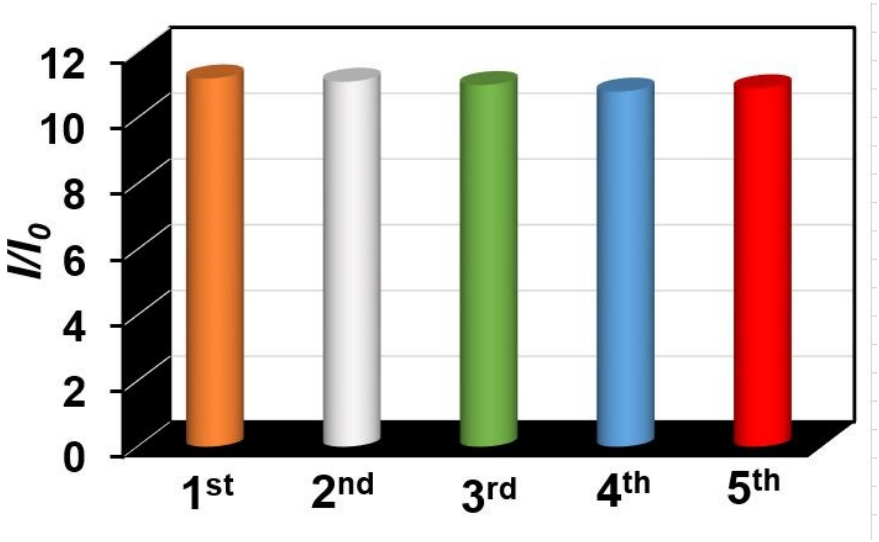

Figure S49. Recyclability test of **1′** towards the sensing of PAA in water.

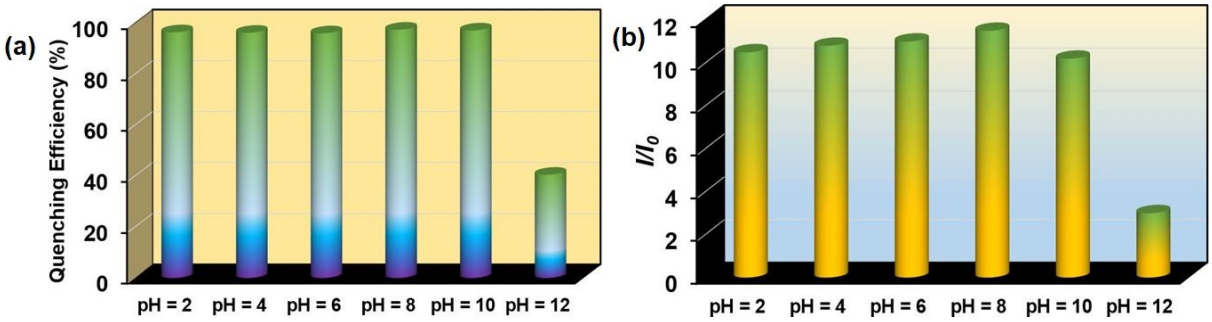

Figure S50. Quenching efficiencies of **1′** after adding 400 µL of 10 mM NX (a) and 5 mM 400 µL PAA (b) solution in different pH solutions (λ_{ex} = 370 nm).

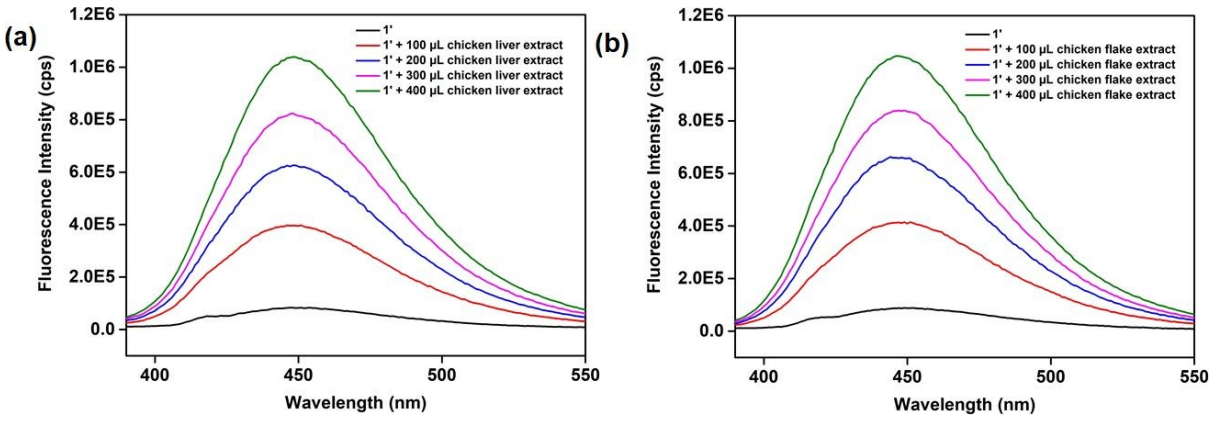

Figure S51. Sensing of PAA in PAA-spiked chicken liver (a) and chicken flake (b) extracts.

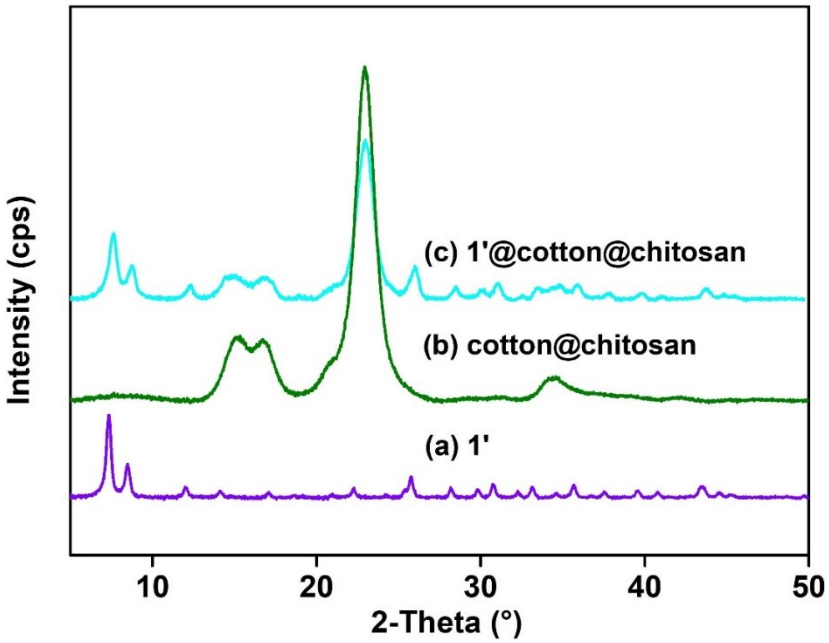

Figure S52. PXRD patterns of (a) compound **1′**, (b) cotton@chitosan and (c) **1′**@cotton@chitosan composite.

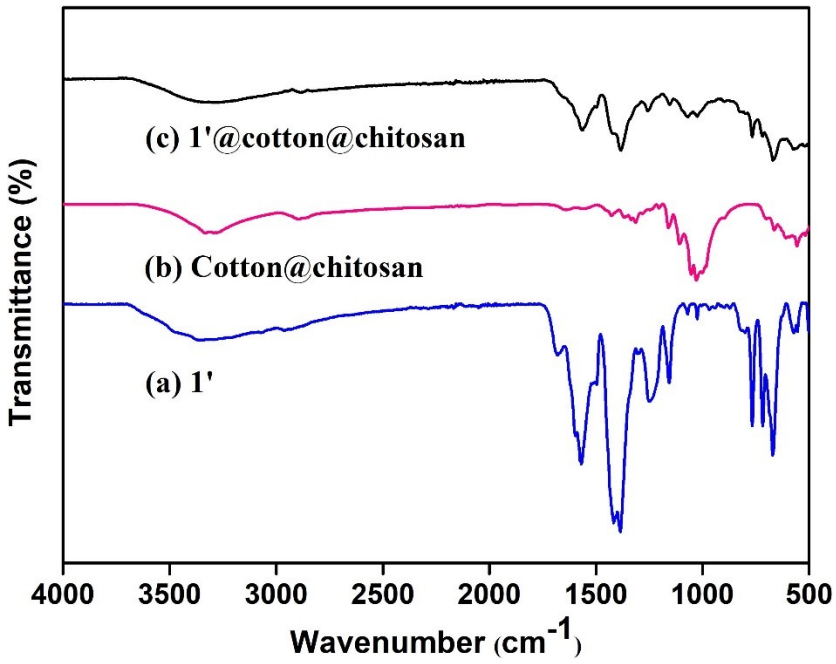

Figure S53. FT-IR spectra of compound (a) **1′**, (b) cotton@chitosan, (c) **1′**@cotton@chitosan composite.

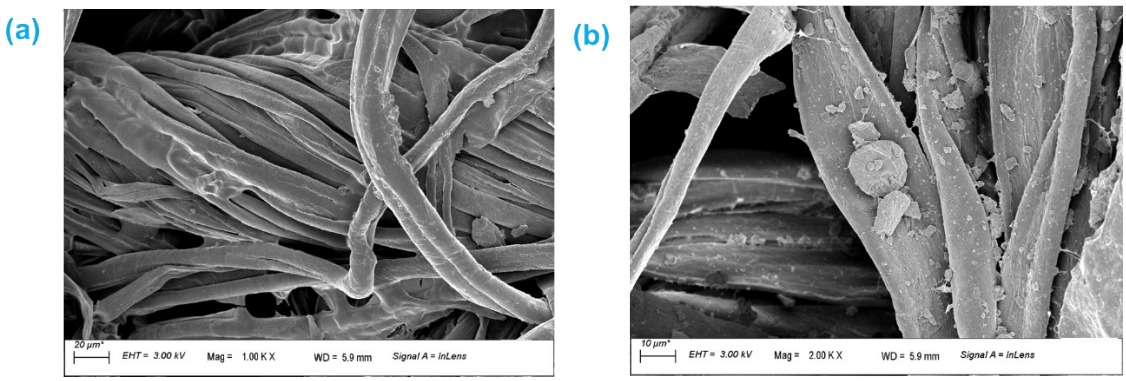

Figure S54. FE-SEM images of (a) cotton@chitosan and (b) **1′**@cotton@chitosan composite.

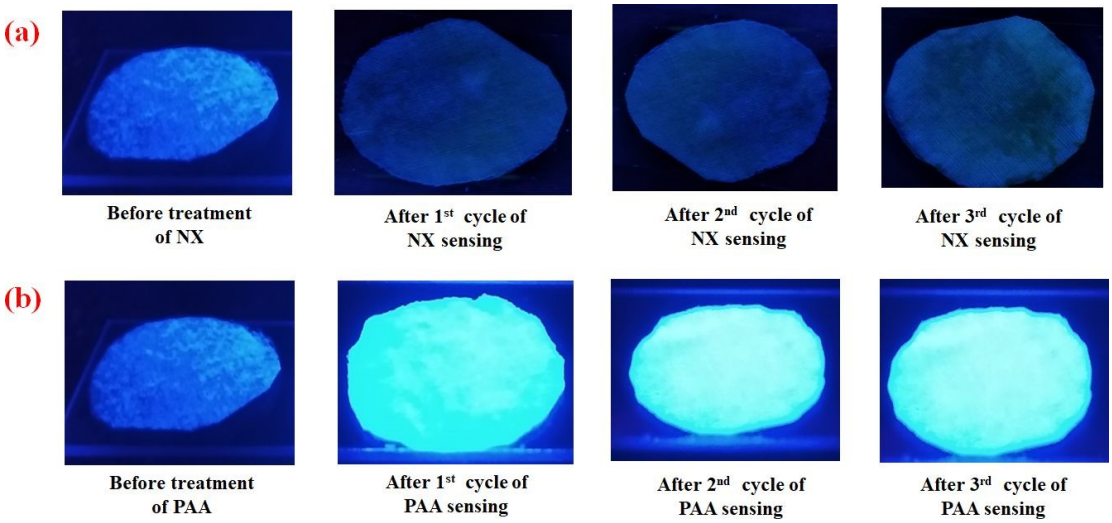

Figure S55. Digital images of **1′**@cotton@chitosan composite after each cycle of sensing of (a) NX and (b) PAA.

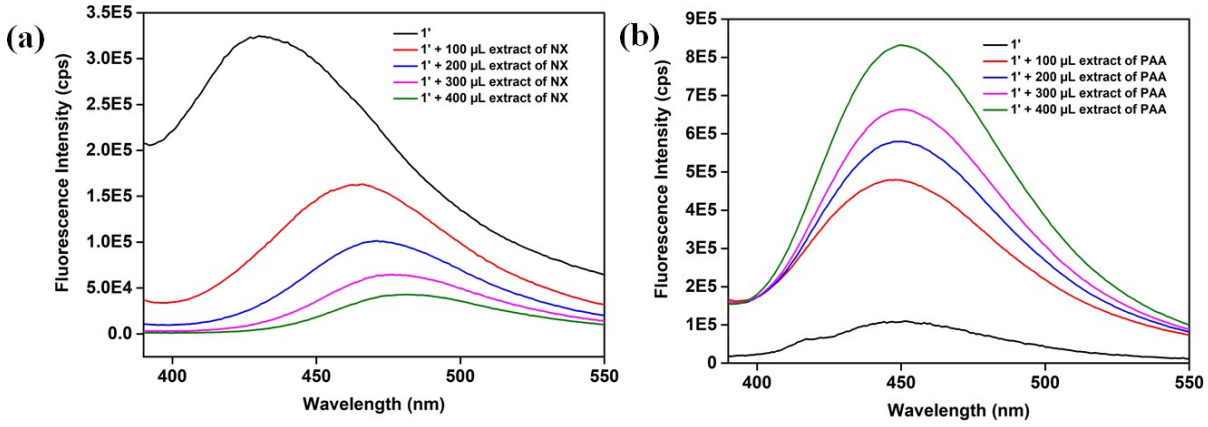

Figure S56. Sensing of (a) NX and (b) PAA after addition of different volume of aqueous extract of soil samples after the treatment of targeted analytes.

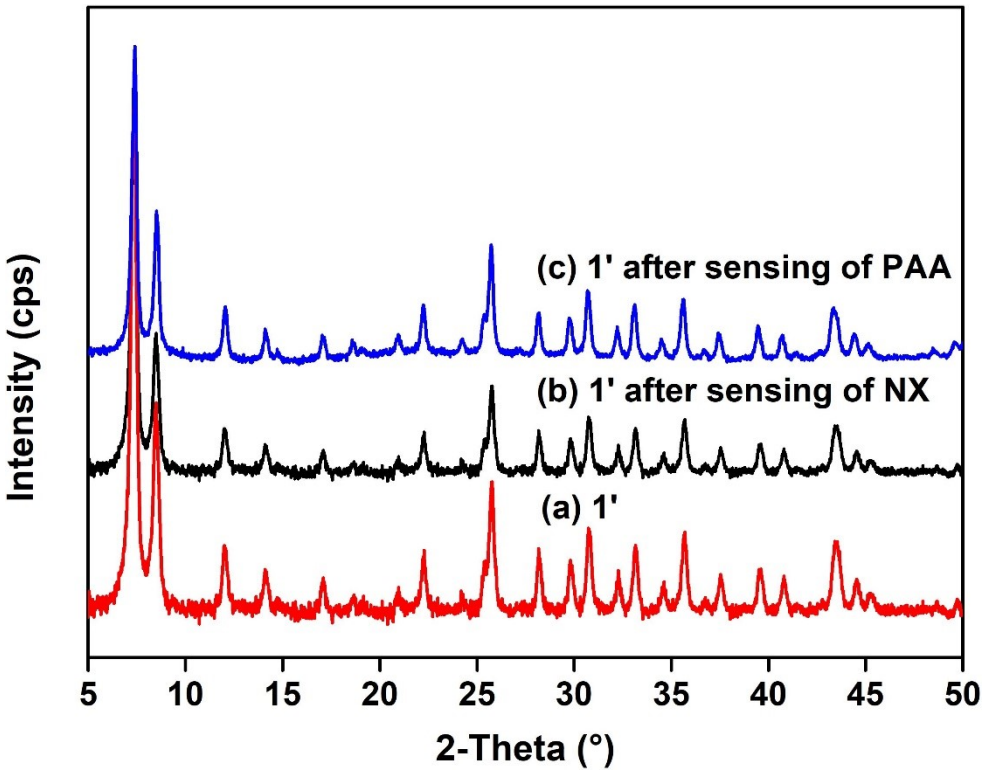

Figure S57. PXRD patterns of compound **1′** before (a) and after treatment with NX (b) and PAA (c) in water.

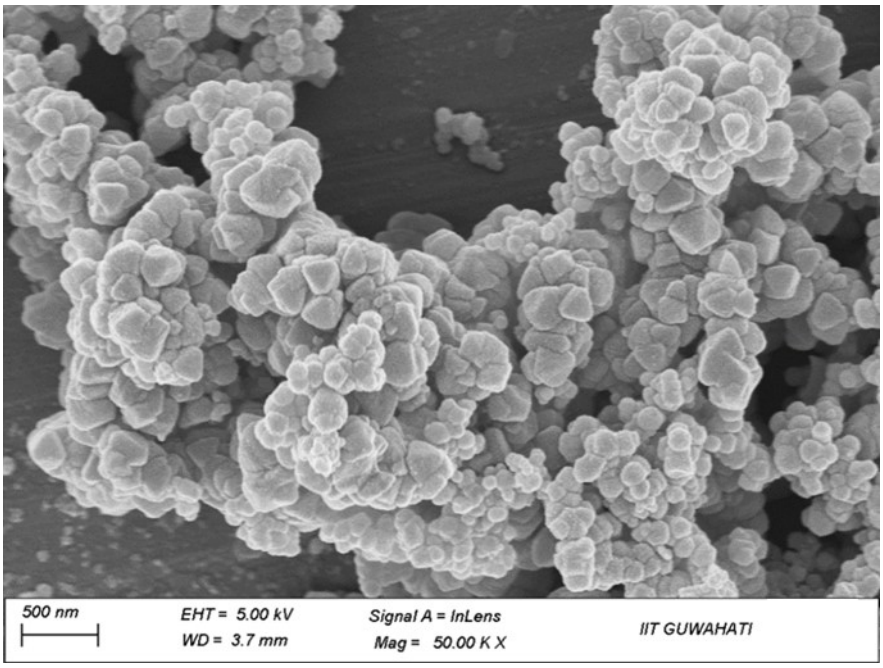

Figure S58. FE-SEM images of **1′** after NX sensing experiment.

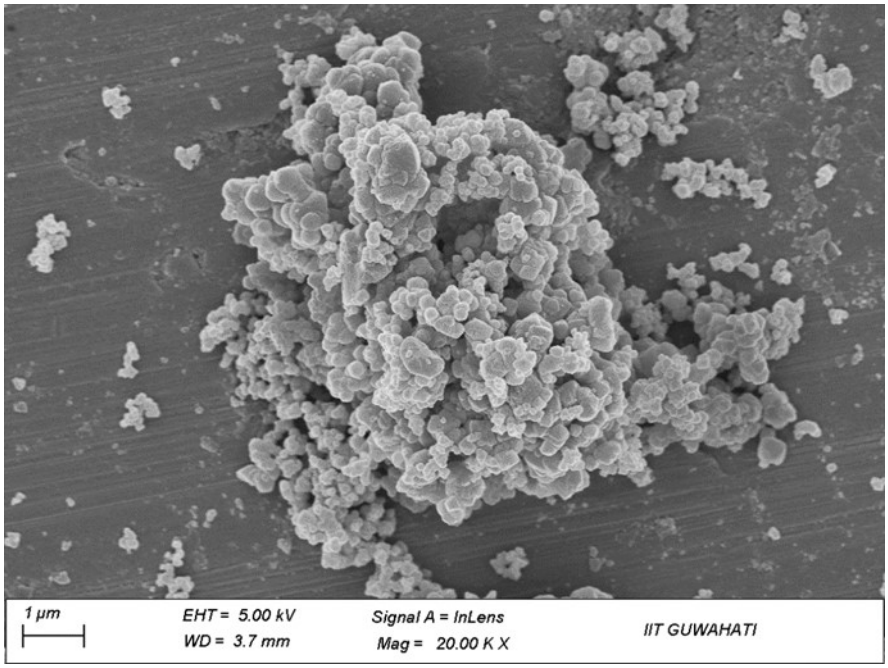

Figure S59. FE-SEM image of **1′** after sensing of PAA in water.

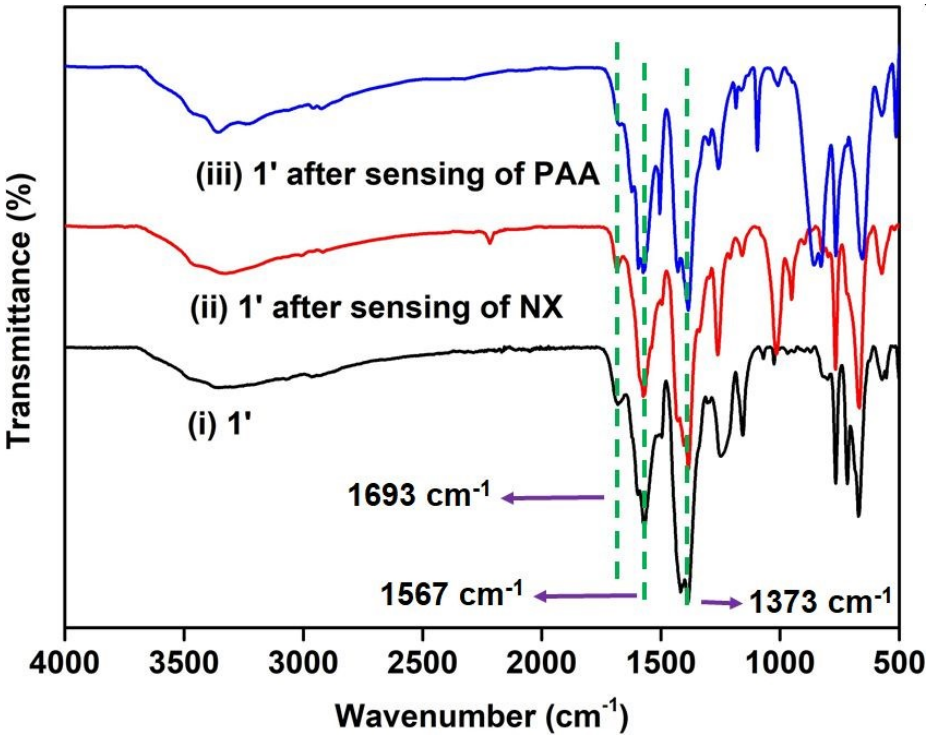

Figure S60. FT-IR spectra of **1′** (a), **1′** after sensing of NX (b) and PAA (c).

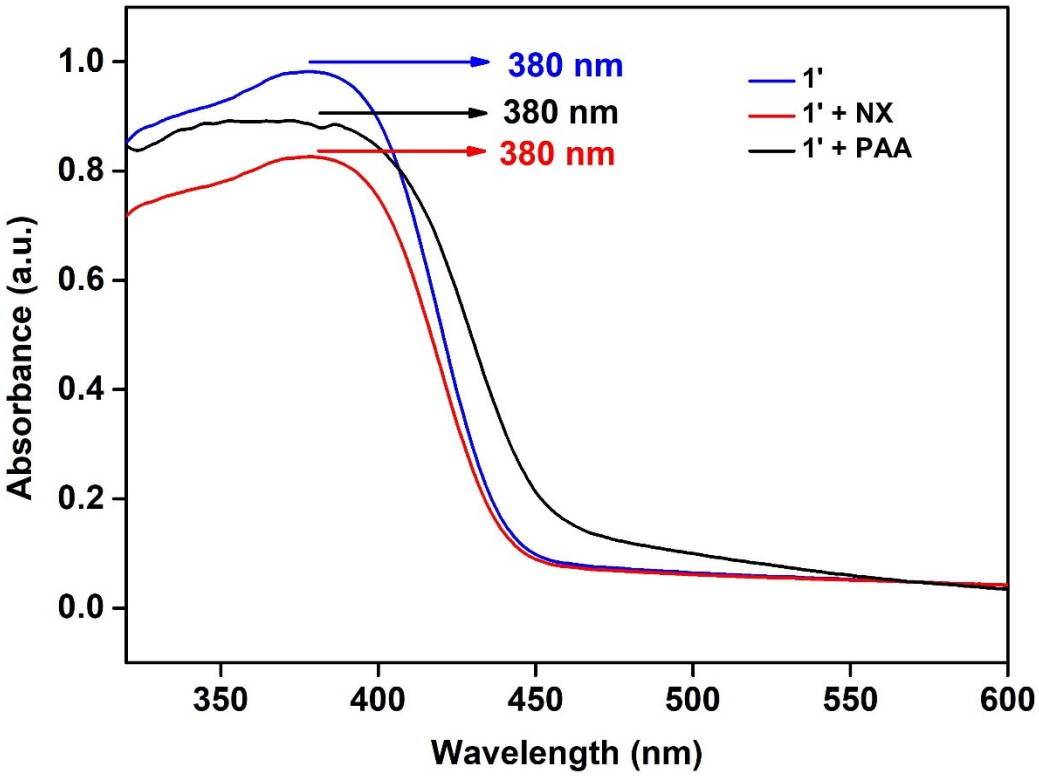

Figure S61. Solid state UV-Vis spectra of **1′** (blue line), **1′** after sensing of NX (red line) and PAA (black line).

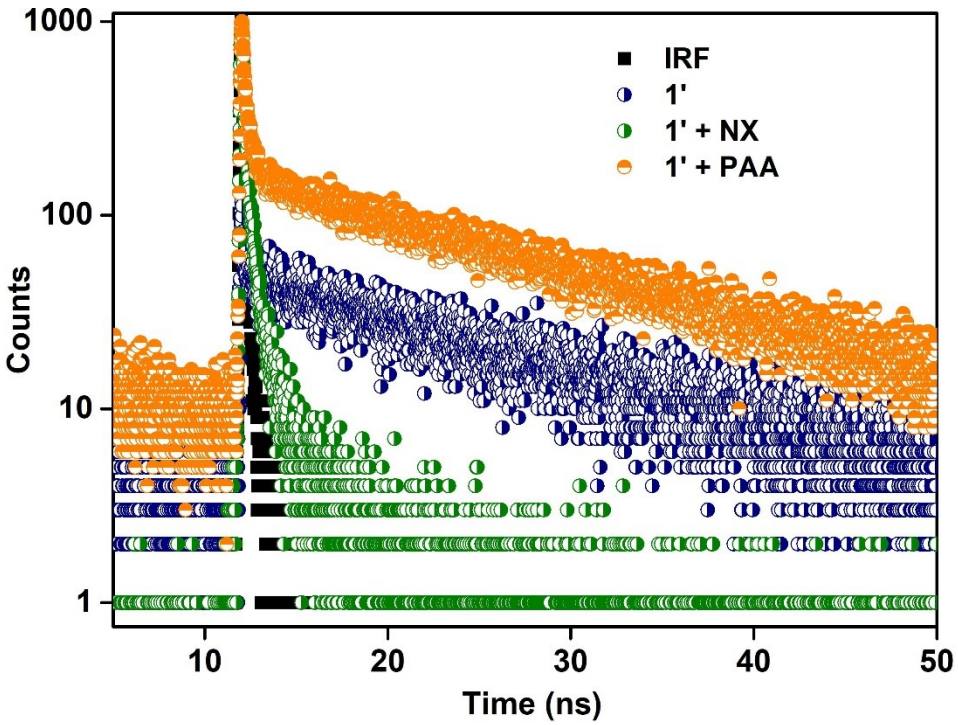

Figure S62. Lifetime decay profile of **1′** in absence and presence of NX and PAA solution (λ_{ex} = 370 nm, monitored at 375 nm). Here, IRF = instrument response function.

Table S1. Fluorescence lifetimes of **1′** before and after the addition of NX solution (λ_{ex} = 375 nm, pulsed diode laser).

Volume of NX Solution Added (μL)	a_1	a_2	τ_1 (ns)	τ_2 (ns)	$<\tau>$* (ns)	χ^2
0	0.31	0.69	0.08	15.21	10.52	1.00
400	0.16	0.84	0.11	1.08	0.92	1.00

* $<\tau> = a_1\tau_1 + a_2\tau_2$

Table S2. Fluorescence lifetimes of **1′** before and after the addition of PAA solution (λ_{ex} = 375 nm, pulsed diode laser).

Volume of PAA solution added (μL)	a_1	a_2	τ_1 (ns)	τ_2 (ns)	$<\tau>$* (ns)	χ^2
0	0.31	0.69	0.08	15.21	10.52	1.00
400	0.10	0.99	0.06	11.87	11.70	1.08

* $<\tau> = a_1\tau_1 + a_2\tau_2$

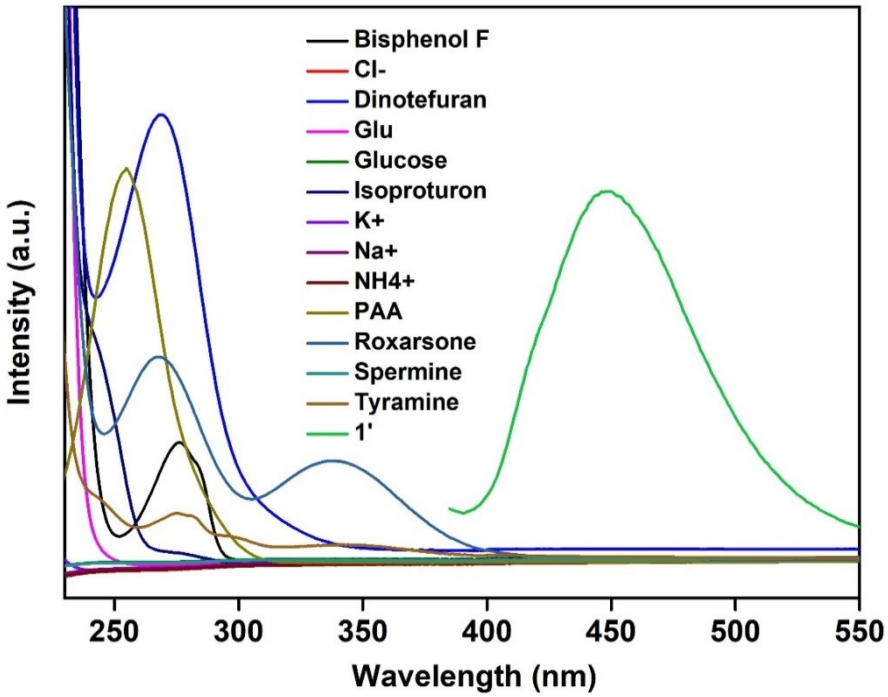

Figure S63. Spectral overlap between emission spectrum of **1′** and absorption spectra of PAA and other analytes.

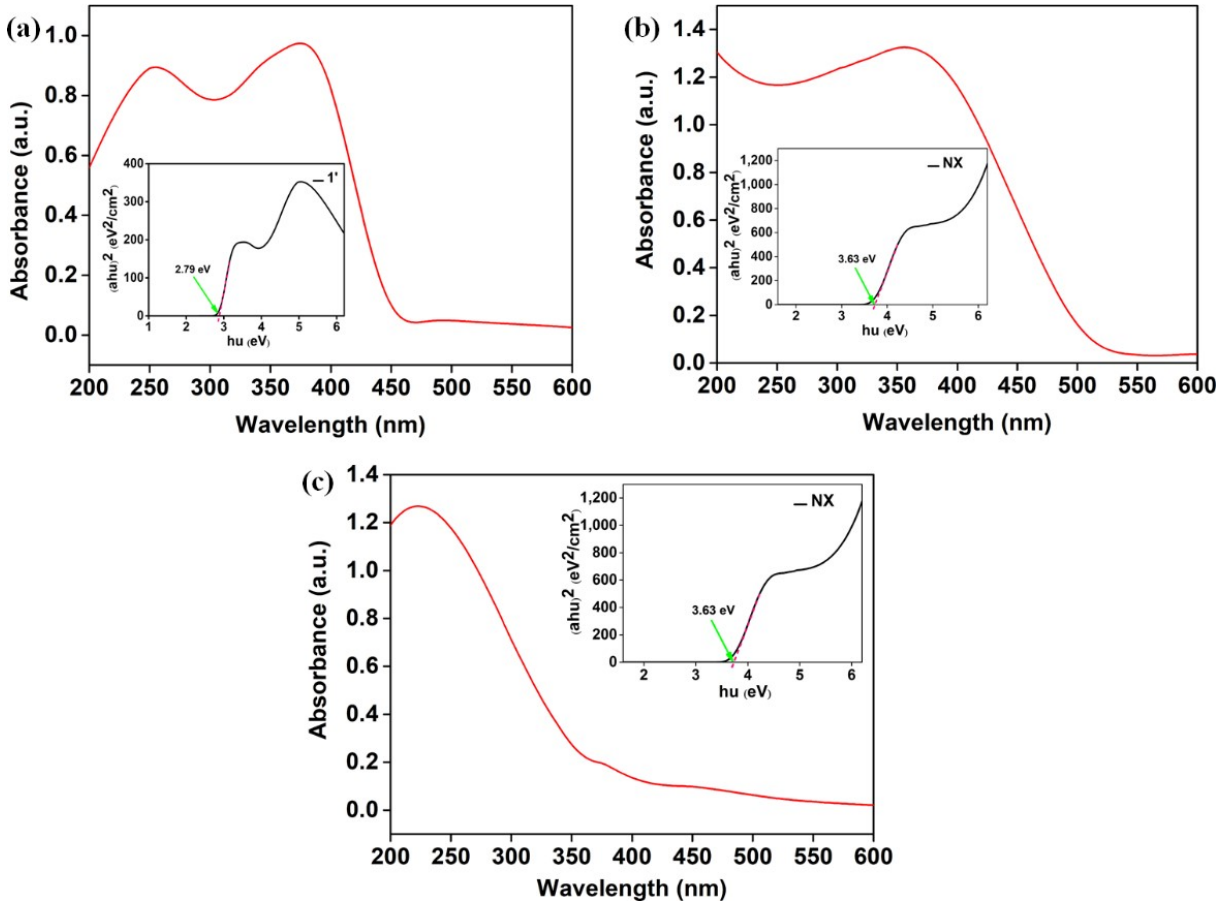

Figure S64. (a) UV-DRS spectra of **1′**, (b) NX and (c) PAA (Tauc plots are shown in insets).

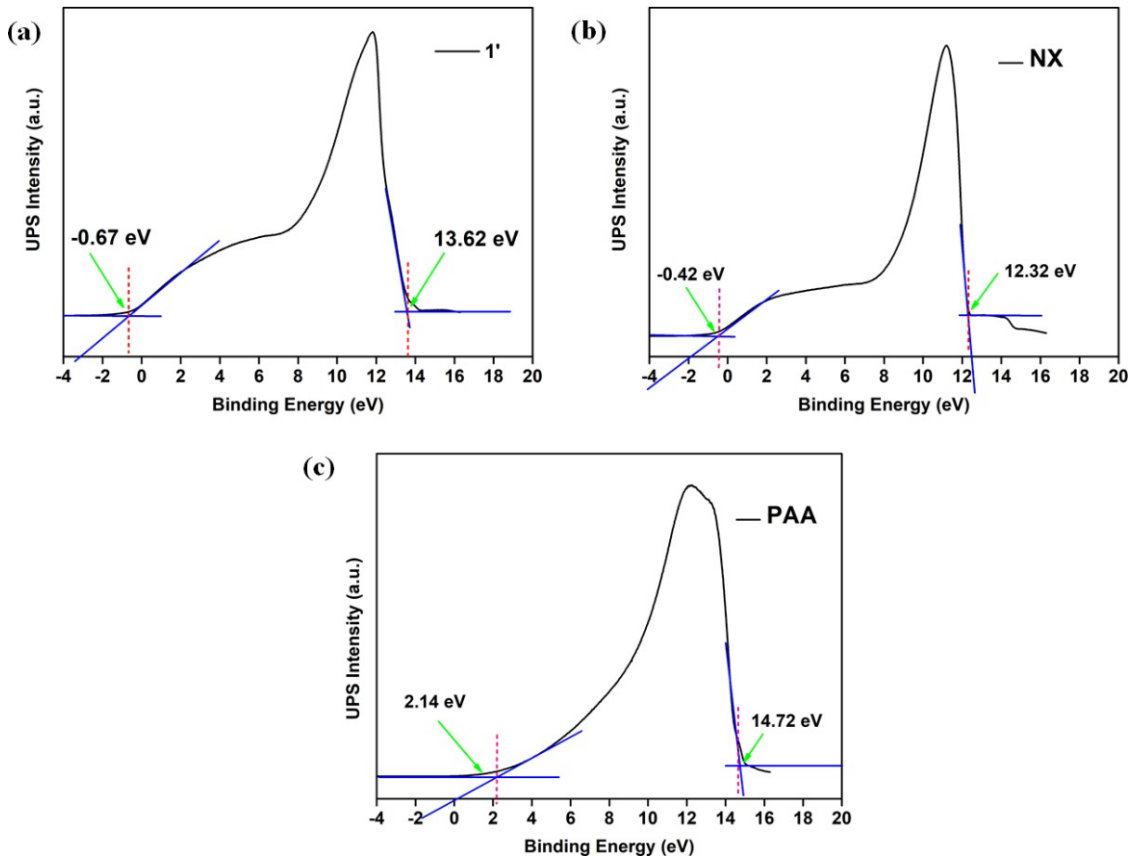

Figure S65. (a) UPS spectra of **1′**, (b) NX and (c) PAA.

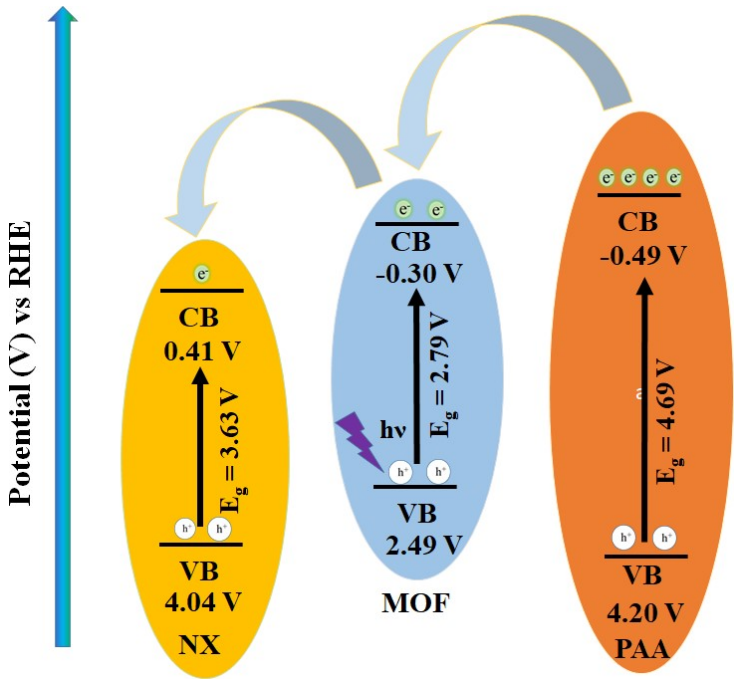

Figure S66. Schematic representation of electron transfers from the CB of **1′** to the CB of NX, and from the CB band of PAA to the CB band of **1′**.

Table S3. Statistical details of different analytical parameters for the sensing of NX by **1′**.

Concentration Range (nM)	Slopes	Intercepts	Correlation Coefficient (R^2)	$S_{y/x}$ [a]	LOD[b] (nM)	LOQ[c] (nM)	Regression Equation
0-44.8	-1321.8	2499661	0.998	14664.6	33.3	110.9	-1321.8x + 2499661
	-1524.4	2508644	0.995	13846.9	27.2	90.8	-1524.4x + 13846.9
	-1434.8	2506305	0.997	12908.2	26.9	89.9	-1434.8x + 2506305
Average	-1427.0	2504870	0.996	13806.6	29.2	97.3	-1427.0x + 2504870
SD	101.5	4660.2	0.002	878.8	3.6	11.8	(-1427.0 ± 101.5)x + (2504870 ± 4660.2)

[a] Standard deviation of the residuals, [b] Limit of detection, [c] Limit of quantification

Table S4. Statistical details of different analytical parameters for the sensing of PAA by **1′**.

Concentration Range (nM)	Slopes	Intercepts	Correlation Coefficient (R^2)	$S_{y/x}$ [a]	LOD[b] (nM)	LOQ[c] (nM)	Regression Equation
0-45	190.4	136762	0.995	1093.4	17.2	57.4	190.4x + 136762
	213.3	136129.1	0.997	1061.5	14.9	49.7	213.3x + 136129.1
	190.0	136624.1	0.998	1234.7	19.5	64.9	190.0x + 136624.1
Average	197.9	136505.1	0.996	1129.9	17.2	57.4	197.9x + 136505.1
SD	13.3	332.8	0.002	92.2	2.3	7.59	(197.9 ± 13.3)x + (136505.1 ± 332.8)

[a] Standard deviation of the residuals, [b] Limit of detection, [c] Limit of quantification

Table S5. Comparison between the spiked and observed concentrations and recovery of NX in different real water specimens.

Type of Water	Spiked Conc. of NX (μM)	Observed Conc. of NX (μM)	Recovery (%)
Milli-Q Water	(i) 1111.1 (ii) 555.5 (iii) 277.7	(i) 1110.0 (ii) 552.4 (iii) 274.6	(i) 99.9 (ii) 99.4 (iii) 98.8
Lake Water	(i) 1111.1 (ii) 555.5 (iii) 277.7	(i) 1101.9 (ii) 552.5 (iii) 274.6	(i) 99.1 (ii) 99.4 (iii) 98.8
Tap Water	(i) 1111.1 (ii) 555.5 (iii) 277.7	(i) 1108.2 (ii) 550.1 (iii) 275.6	(i) 99.7 (ii) 99.0 (iii) 99.2
River Water	(i) 1111.1 (ii) 555.5 (iii) 277.7	(i) 1104.2 (ii) 551.2 (iii) 276.7	(i) 99.4 (ii) 99.2 (iii) 99.6

Table S6. Detection of NX in serum samples.

NX Spiked (mol L^{-1})	NX Found (mol L^{-1})	Recovery (%)	RSD (%) (n=3)
38.8	35.5	91.5	1.3
114.5	112.9	98.6	2.0
187.9	180.5	96.1	1.8

Table S7. Detection of NX in urine samples.

NX Spiked (mol L^{-1})	NX Found (mol L^{-1})	Recovery (%)	RSD (%) (n=3)
38.8	36.7	94.6	3.1
114.5	111.5	97.4	3.0
187.9	183.6	97.7	1.1

Table S8. Comparison between the spiked and observed concentrations and recovery of PAA in different real water specimens.

Type of Water	Spiked Conc. of PAA (mM)	Observed Conc. of PAA (mM)	Recovery (%)
Milli-Q Water	(i) 555.5 (ii) 277.7 (iii) 111.1	(i) 550.2 (ii) 270.1 (iii) 110.1	(i) 99.0 (ii) 97.3 (iii) 99.1
Lake Water	(i) 555.5 (ii) 277.7 (iii) 111.1	(i) 549.9 (ii) 271.2 (iii) 105.0	(i) 98.9 (ii) 97.6 (iii) 94.5
Tap Water	(i) 555.5 (ii) 277.7 (iii) 111.1	(i) 557.5 (ii) 282.9 (iii) 116.1	(i) 100.4 (ii) 101.8 (iii) 104.5
River Water	(i) 555.5 (ii) 277.7 (iii) 111.1	(i) 560.2 (ii) 276.1 (iii) 108.9	(i) 100.8 (ii) 99.6 (iii) 98.0

Table S9. Evaluation of intra-day, inter-day accuracy and precision study of change in fluorescence intensity of **1′** after incremental addition of 10 mM aqueous solution of NX.

Parameter	Amount of NX Added (μL)	Fluorescence Intensity (cps) at λ_{max} = 448 nm			Average PL Intensity (cps)	SD	RE%
Repeatability Intra-day precision	0	423797.3	422948.9	422232.5	422992.9	783.3	-0.190
	100	88161.3	90315.41	92781.84	90419.51	2312.0	2.497
	200	46171.6	48488.65	49677.1	48112.44	1782.7	4.034
	300	20883.4	22001.45	23383.94	22089.61	1252.5	5.460
	400	8310.3	8695.467	9236.896	8747.558	465.5	4.998
Reproducibility Inter-day precision	0	423797.3	421503.4	420115.1	421805.2	1859.6	0.472
	100	88161.3	94417.14	96230.0	92936.1	4233.3	5.137
	200	46171.6	52490.56	53982.3	50881.5	4146.5	9.256
	300	20883.4	24814.98	26179.0	239599.1	2749.6	1.2
	400	8310.6	10111.86	10111.8	10956.8	9793.7	1.5

Table S10. Evaluation of intra-day, inter-day accuracy and precision study of change in fluorescence intensity of **1′** after incremental addition of 5 mM aqueous solution of PAA.

Parameter	Amount of PAA added (μL)	Fluorescence Intensity (cps) at λ_{max} = 448 nm			Average PL Intensity (cps)	SD	RE%
Repeatability Intra-day precision	0	107534.6	107670	109788.4	108331	1263.9	0.007
	100	529078.7	528523.5	524517.3	527373.1	2488.8	0.003
	200	759659.9	762164.3	761487.2	761103.8	1295.4	0.001
	300	973368.1	985280.8	980433.4	979694.1	5990.6	0.006
	400	1124000	1115240	1121770	1120337	4552.5	0.003
Reproducibility Inter-day precision	0	109788.4	109889.4	107616.9	109098.2	1283.8	0.006
	100	524517.3	521278.9	518373.4	521389.9	3073.4	0.006
	200	761487.2	750112.6	754648.9	755416.2	5726.0	0.008
	300	980433.4	972889.5	972752.1	975358.3	4395.6	0.005
	400	1121770	1112910	1109190	1114623	6462.6	0.006

Table S11. Unit cell parameters of **1′** obtained by indexing its PXRD data. The obtained values have been compared with parent MOF.

Compound Name	Compound **1′**	UiO-66[1]
Crystal System	cubic	cubic
a = b = c (Å)	20.745 (10)	20.700 (2)
V (Å^3)	8927.7 (35)	8870.3 (2)

Table S12. Comparison of fluorescence sensing results using **1′** in different solvent media.

Sl. No.	Solvent Used	Quenching Efficiency After Addition of Nitroxinil (%)	Fold-Increments After Addition of p-Arsanilic Acid
1	water	99	11.2
2	acetonitrile	87.7	1.30
3	methanol	80.7	1.32
4	DMF	92	1.10

Table S13. Comparison of the detection performance of present probe (**1′**) with some previously reported probes of NX.

Sl. No.	Sensor Material	Type of Material	Sensing Medium	Detection Limit	Response Time	Detection Method	Ref.
1	graphite powder, paraffin oil	carbon paste electrode	water	3.1×10^{-7} M	20 s	voltammetry	2
2	(i) single–walled carbon nanotubes (ii) graphene (iii) carbon nanohorns	GCE	water, acetonitrile	(i) 0.36×10^{-6} M (ii) 0.11×10^{-6} M (iii) 0.34×10^{-6} M	> 30 s	voltammetry	3
3	mercury	electrode	BR buffer of pH 1.9-11 containing 20% (v/v) ethanol	1.31×10^{-8} M	> 6 min	differential-pulse adsorptive stripping voltammetry	4
4	albumin-dye	multilayered composite	water	~8.7 ppb	<10 s	fluorometry by molecular docking	5
5	**$[Hf_6O_4(OH)_4(C_9H_5NO_5)_6]$ (1′)**	**MOF**	**water**	**11.8 nM**	**5 s**	fluorometry	**this work**

Table S14. Comparison of the detection performance of present probe (**1′**) with some previously reported probes of PAA.

Sl. No.	Sensor Material	Type of Material	Sensing Medium	Detection Limit	Response Time	Detection Method	Ref.
1	Cu(I)-tpp@ZIF-8	MOF	water	0.4 μg·L^{-1}	-	fluorometry	6
2	Cu(II)-tpt-on-Cu(I)-tpt membrane	MOF-on-MOF	water	0.0556 μg L^{-1}	-	fluorometry	7
3	$[Eu_2(clhex)\cdot 2H_2O)]\cdot H_2O$	MOF-on-MOF	water	1.81 μM	>5 min	fluorometry	8
4	PCN-224/rGO	nano-composite	water	5.47 ng L^{-1}	>2 h	photoelectrochemistry	9
5	zirconium oxide	nano-structure	water	< 50 μg·L^{-1}	-	hyper-cross-linked anion exchange	10
6	**$[Hf_6O_4(OH)_4(C_9H_5NO_5)_6]$ (1′)**	**MOF**	**water**	**17.2 nM**	**15 s**	**fluorometry**	**this work**

References:

1. J. H. Cavka, S. Jakobsen, U. Olsbye, N. Guillou, C. Lamberti, S. Bordiga and K. P. Lillerud, *J. Am. Chem. Soc.*, 2008, **130**, 13850-13851.
2. M. M. Salim, S. Ashraf, H. M. Hashem and F. Belal, *Sci. Rep.*, 2022, **12**, 14289.
3. K. Sipa, M. Brycht, A. Leniart and S. Skrzypek, *J. Electroanal. Chem.*, 2019, **848**, 113294.
4. M. Ghoneim, M. El-Ries, A. a. Hassanein and A. Abd-Elaziz, *J. Pharm. Biomed. Anal.*, 2006, **41**, 1268-1273.
5. M. Zhou, C. Song, T. Qin, Z. Xun and B. Liu, *Spectrochim. Acta A Mol.*, 2023, 122974.
6. K. Zhu, J. Wu, R. Fan, Y. Cao, H. Lu, B. Wang, X. Zheng, Y. Yin, P. Wang and Y. Yang, *Chem. Eng. J.*, 2022, **427**, 131483.
7. K. Zhu, R. Fan, J. Wu, B. Wang, H. Lu, X. Zheng, T. Sun, S. Gai, X. Zhou and Y. Yang, *ACS Appl. Mater. Interfaces.*, 2020, **12**, 58239-58251.
8. C. Y. Wang, H. Fu, P. Wang and C. C. Wang, *Appl. Organomet. Chem.*, 2019, **33**, e5021.
9. M. Peng, G. Guan, H. Deng, B. Han, C. Tian, J. Zhuang, Y. Xu, W. Liu and Z. Lin, *Environ. Sci. Nano*, 2019, **6**, 207-215.
10. Z. Zhao, P. Wu, Z. Fang and X. Zhang, *Chem. Eng. J.*, 2020, **391**, 123624.